TECHNICAL MEMORANDUM

587

GEMS data assimilation system for chemically reactive gases

Antje Inness, Johannes Flemming,
Martin Suttie and Luke Jones

Research Department

May 2009

European Centre for Medium-Range Weather Forecasts
Europäisches Zentrum für mittelfristige Wettervorhersage
Centre européen pour les prévisions météorologiques à moyen

Series: ECMWF Technical Memoranda

A full list of ECMWF Publications can be found on our web site under:
http://www.ecmwf.int/publications/

Contact: library@ecmwf.int

European Centre for Medium-Range Weather Forecasts
Shinfield Park, Reading, RG2 9AX, England

Abstract

A data assimilation system for chemically reactive gases has been developed at the European Centre for Medium-Range Weather Forecasts (ECMWF) for the "Global and regional Earth-system Monitoring using Satellite and in-situ data" (GEMS) project. ECMWF's integrated forecast system (IFS) was extended to include the chemically reactive gases ozone, carbon monoxide, nitrogen oxides, formaldehyde and sulphur dioxide. Chemical transport models were coupled to the IFS using the OASIS4 coupler to model the chemical processes and to provide the IFS with chemical production and loss rates. This paper describes the assimilation system for the reactive gases, presents the background error statistics developed for the reactive gases, and shows some first results of the assimilation of satellite retrievals for all five new species.

1 Introduction

The EU-funded GEMS (Global and regional Earth-system Monitoring using Satellite and in-situ data) project is developing a comprehensive data analysis and modelling system for monitoring the global distribution of atmospheric constituents important for climate, air quality and UV radiation, with a focus on Europe. As part of the project a pre-operational data assimilation and forecasting system for aerosols, greenhouse gases and chemically reactive gases has been developed by extending ECMWF's Integrated Forecast System (IFS), allowing ECMWF's 4D-VAR data assimilation system to be used to assimilate satellite observations of atmospheric composition at global scale (Hollingsworth et al. 2008).

This paper focuses on the assimilation system for chemically reactive gases developed under the global reactive gases (GRG) subproject of GEMS. Information about the aerosol subproject can be found in Benedetti et al. (2009) and about the greenhouse gases subproject in Engelen et al. (2009). The GRG subproject focuses on the assimilation of the following gases: Ozone (O_3), carbon monoxide (CO), nitrogen oxides (NOx = NO + NO_2), formaldehyde (HCHO) and sulphur dioxide (SO_2). These gases play a key role in the chemistry of the atmosphere and are observable from space.

Ozone is crucially important for the chemistry of the troposphere. Tropospheric ozone is a regional scale pollutant and at high concentrations near the surface, it is harmful to humans and vegetation (National Research Council 1991). Photolysis of ozone, followed by reaction with water vapour, provides the primary source of the hydroxyl radical (OH), the main atmospheric oxidant, in the troposphere (e.g. Logan et al. 1981). Ozone is also a significant greenhouse gas, particularly in the upper troposphere (Hansen et al. 1997). The majority of tropospheric ozone formation occurs when NOx, CO, and volatile organic compounds (VOCs) react in the atmosphere in the presence of sunlight. These ozone precursors are emitted by traffic and industrial activities. In urban areas in the Northern Hemisphere (NH), high ozone levels usually occur during the summer.

CO is one of the most important trace gases in the troposphere and affects the concentrations of the OH radical. CO has natural and anthropogenic sources (see reviews by Seinfeld and Randis (2006) and Kanakidou and Crutzen (1999)). It is emitted from the soil, plants and the ocean, but the main sources of CO are incomplete fossil fuel and biomass burning, which lead to enhanced surface concentrations. The highest CO concentrations are found over the industrial regions of Europe, Asia and North America. Surface concentrations are higher during the winter than during the summer months because of the shorter lifetime in the summer due to higher OH concentrations and more intense mixing processes. Tropical biomass burning is most intense during the dry season (December-April in the NH tropics, July-October in SH tropics). CO has a lifetime of a few months and can serve as a tracer for regional and inter-continental transport of polluted air.

NOx plays a key role in tropospheric chemistry and is the main ingredient in the formation of ground level ozone. Its sources are anthropogenic emission (traffic, industry, power plants), biomass burning (Crutzen and Schmailzl 1983), soil emissions (Granli and Bokman 1994) and lightning (Martin et al. 2007). NOx has a

lifetime of a few days or less in the boundary layer, so that concentrations are larger over land than over the cleaner oceans. The largest concentrations are found over industrial and urban regions of the Eastern US, California, Europe, China and Japan.

HCHO is one of the most abundant hydrocarbons in the atmosphere. It is formed in most Non-Methane hydrocarbon (NMHC) oxidation chains. Its primary emission sources are industrial activities, and fossil fuel and biomass burning. The largest contribution to the HCHO budget is its large secondary source from the oxidation of VOCs (Atkinson 1994), the main precursors being methane and isoprene. The main sinks of HCHO are photolysis and oxidation by OH. HCHO has a short lifetime of a few hours, making it a good indicator of hydrocarbon emission areas.

SO_2 contributes to acid rain and is a key precursor for sulphuric acid aerosol formation. At high concentrations, it can affect human health, in particular in combination with fog (smog). Anthropogenic activities such as fossil fuel burning and metal smelting have raised atmospheric SO_2 concentrations by up to 3 orders of magnitude over the last century (Pham et al. 1996). Another source for SO_2 are volcanic eruptions that can eject large amounts of SO_2 into the atmosphere. The ash and SO_2 emitted by volcanic eruptions are a major hazard to aviation. In the troposphere SO_2 has a lifetime of a few days, in the stratosphere several weeks.

For the assimilation of tropospheric reactive gases it is important to have a complex chemistry scheme in the model and assimilation system, so that chemical source and sink processes can be accounted for. For the GEMS system it was deemed premature and numerically too expensive to include a complex chemistry scheme in the IFS. Instead, chemical transport models (CTMs) coupled to the IFS are used to provide the chemical tendencies for the IFS. The OASIS4 coupler (Valcke and Redler 2006) is used to couple the three CTMs MOZART (Kinnison et al. 2007; Horowitz et al. 2003), MOCAGE (Josse et al. 2004) and TM5 (Krol et al. 2005) to the IFS. Any one of these CTMs can then be used to provide chemical production and loss rates for the GRG fields to the IFS. The CTM in turn is driven by meteorological fields from the IFS. The reactive gases included in the IFS can then be restrained by the assimilation of satellite data from various instruments.

This paper describes the GEMS reactive gases data assimilation system and shows some first results from the assimilation of O_3, CO, NOx, HCHO, and SO_2 satellite data with the coupled GEMS system.

2 Coupled IFS GRG system

The GEMS data assimilation system for chemically reactive gases was constructed by extending ECMWF's integrated forecast system (IFS) to include fields for O_3, CO, NOx, HCHO, and SO_2. Chemical production and loss rates (chemical tendencies) for these gases are supplied by a CTM that is coupled to the IFS using the OASIS4 coupler. Technically, it is possible to couple any one of the three CTMs MOZART, MOCAGE and TM5 to the IFS. The IFS supplies the meteorological data to the CTM every hour, and the CTM provides IFS with initial conditions for the tracers and with three dimensional tendency fields every hour.

The reactive gas O_3 had already been included in the IFS as an additional model variable, and ozone data have been assimilated at ECMWF since 1999 (Hólm et al. 1999, Dethof and Hólm 2004). However, the ECMWF approach differes from the GEMS approach because it uses an inbuilt chemistry routine with a parametrization of photochemical sources and sinces based on an updated version of Cariolle and Déqué (1999) instead if a coupled CTM to provied the chemical tendencies.

All the experiments described in this paper use a setup where the MOZART CTM is coupled to the IFS with a coupling frequency of 1 hour. This CTM was chosen because it is the numerically least expensive one of the three CTMs, and it is not feasible to run long assimilation experiments with a numerically more expensive CTM. A description of the MOZART CTM as implemented in the GEMS system can be found in Stein (2009).

2.1 Data assimilation

2.1.1 4D-Var

ECMWF has used an incremental formulation of 4-dimensional variational data assimilation (4D-Var) since 1997. In 4D-Var a cost function is minimized to combine the model background and the observations to obtain the best possible forecast by adjusting the initial conditions. In its incremental formulation (Courtier et al. 1994) 4D-Var can be written as

$$J(\delta x) = \frac{1}{2}\delta x^T B^{-1}\delta x + \frac{1}{2}(H\delta x - d)^T R^{-1}(H\delta x - d), \quad (1)$$

where δx is the increment, B the background error covariance matrix, R the observation error covariance matrix (comprising of observational and representativeness errors), and H a linear approximation of the observation operator. $d = y - Hx_b$ is the innovation vector, y the observation vector and x_b the background.

The GRG fields are fully integrated into the ECMWF variational analysis as additional model variables. They are minimized together with the main ECMWF fields, which means they can, in priciple, influence the analysis of wind and other meteorological variables in 4D-Var. However, given the uncertainty of the GRG observations and the lack of observational constraints of variables such as wind or temperature in the stratosphere and mesosphere, a possible influence of the GRG observations on the meteorological fields is currently suppressed.

2.1.2 Background errors for the reactive gases

In the ECMWF data assimilation system the background error covariance matrix is given in a wavelet formulation (Fisher 2004, 2006). This allows both spatial and spectral variations of the horizontal and vertical background error covariances. The background error correlations used for the ECMWF variables were derived from an ensemble of forecast difference, using a method proposed by Fisher and Andersson (2001).

The standard deviations determine the relative weight of the background in the analysis, the correlations determine how the analysis increments are spread in the horizontal and in the vertical. This is particularly important for vertically integrated observations, such as total column observation. In this case the vertical structure of the increments is entirely determined by the vertical correlations of the background errors since the observations do not give information about this distribution.

The GRG background errors are univariate in order to minimize the feedback effects of the GRG fields on the other variables. For the GEMS ozone field the IFS ozone background error statistics obtained by the ensemble method are used. These are the same background error statistics that are used in ECMWF's operational ozone assimilation. Figure 1 shows vertical profiles of the standard deviation, and the horizontal and vertical correlations of the ozone background errors at 50°N, 10°E.

A different method had to be chosen to determine background error statistics for the other GRG fields because they had not been included in the ensemble of forecast runs. The NMC method (Parrish and Derber 1992) was used to derive initial background error statistics for the reactive gases. For this, 150 days of 2-day forecasts were run with the coupled system initialized from fields produced by the free running MOZART CTM, and the differences between 24-h and 48-h forecasts valid at the same time were used as a proxy for the background errors. These differences were then used to construct a wavelet background error covariance matrix according to the method described by Fisher (2004, 2006). This background error covariance matrix contains the statistics for the reactive gases as well as the original statistics for the other meteorological fields.

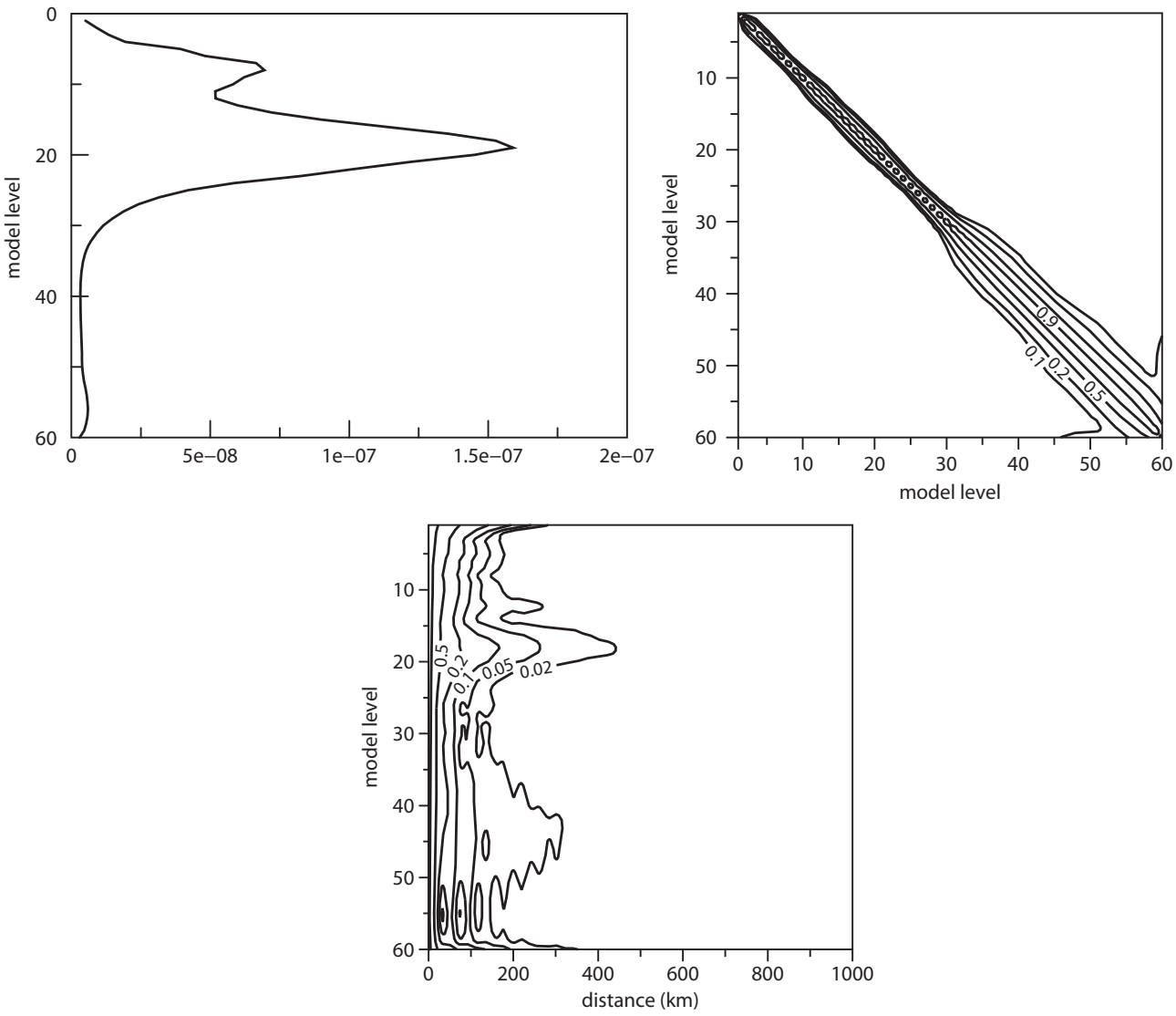

Figure 1: Ozone background error standard deviation profile (top left) in kg/kg, vertical correlations of ozone background errors (top right), and horizontal correlations of ozone background errors (bottom) at 50°N,10°E.

The background error statistics for CO were determined with the NMC method. Figure 2 shows vertical profiles of the standard deviation of the CO background errors and the horizontal and vertical correlations of the background errors for CO at 50°N, 10°E. The standard deviation values in model levels 1 to 19 were set to the value of level 20 to prevent large increments near the model top.

The background errors for HCHO calculated with the NMC method had long horizontal correlations that led to unrealistic increments far away from observations, for example over the polar regions. Therefore the statistics obtained with the NMC method were modified, and a globally constant standard deviation profile was used for HCHO. This was taken from the NMC statistics at 0° latitude, 0° longitude. The background error standard deviations were multiplied by a factor 10, because the values obtained with the NMC method were too small and did not give reasonable HCHO increments in single observation experiments. A diagonal vertical correlation matrix was used, and a prescribed structure function with a length scale of 150 km was used for the horizonal correlations. The HCHO background error standard deviation profile is shown in Figure 3 (left plot).

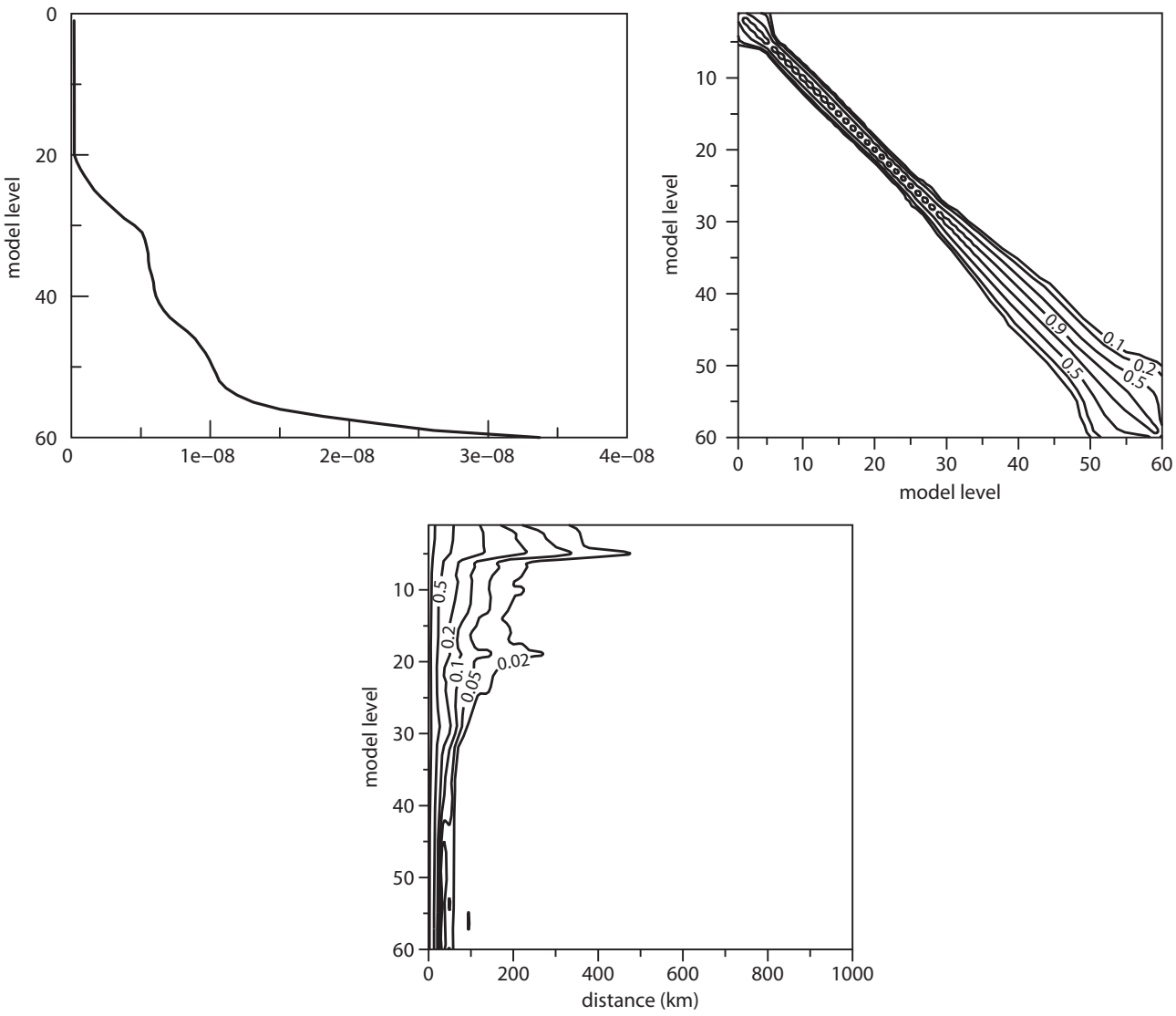

Figure 2: CO background error standard deviation profile (top left) in kg/kg, vertical correlations of CO background errors at (top right), and horizontal correlations of CO background errors (bottom) at 50° N, 10° E.

For the assimilation of NOx data it was found that the analysis based on mixing ratio was prone to large extrapolation errors, due to the high variability of NOx in space and time and the difficulties in modeling the error covariances. Therefore a logarithmic control variable was developed for NOx. The NMC statistics for NOx were calculated from the differences of the natural logarithm of the 24h and 48h forecast fields. Like in the case of HCHO, long horizontal correlations led to unrealistic increments far away from observations, and a globally constant standard deviation profile was used (NMC statistics at 0° latitude, 0° longitude) together with a diagonal vertical correlation matrix, and a prescribed structure function with a length scale of 150 km for the horizonal correlations. The standard deviation profile of the LOG NOx statistics are shown in Figure3 (right plot).

SO_2 observations are only assimilated in the GEMS system in the event of large volcanic eruptions, i.e. when the observed SO_2 concentrations are considerably larger than the atmospheric background values. An NMC approach would not give useful background error statistics for SO_2 for these cases as the forecast model does not have information about individual volcanic eruptions, even though it includes a subaerial volcano emissions

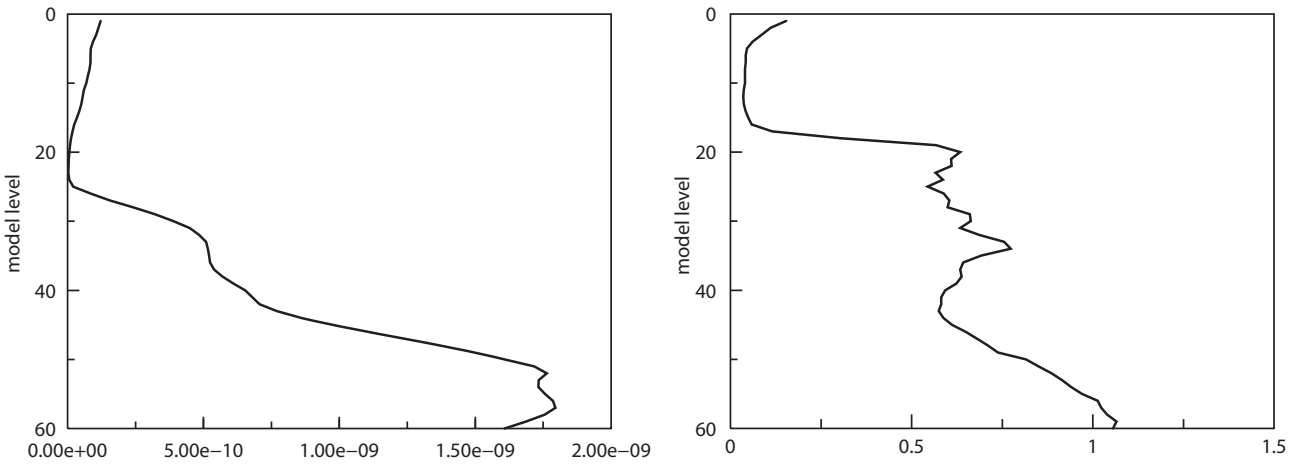

Figure 3: Vertical profiles of the background error standard deviation for HCHO (left) in kg/kg and and NOx (right), dimensionless.

climatology. Therefore, background error statistics for SO_2 were constructed by prescribing a background error standard deviation profile that peaks at model level 36 and 37, corresponding to an SO_2 injection height of about 6 km (see Figure 4). A diagonal vertical correlation matrix, and a prescribed structure function with length scale of 150 km for the horizonal correlations are used SO_2 as for NOx and HCHO.

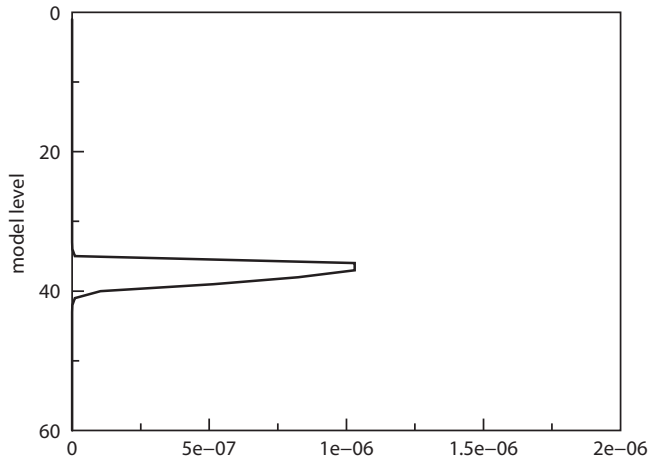

Figure 4: Profile of background error standard deviation for volcanic SO_2 in kg/kg for an injection height of 6 km (left).

2.1.3 Observation errors for reactive gases

The observation error and background error covariance matrices determine the relative weight given to the observation and the background in the analysis. For the reactive gases observation errors given by the data providers are used. If this value is below 5%, a minimum value of 5% is taken. The observation error is assumed to include a representativeness error that arises because of differences in resolution of observation and the model, and that accounts for scales unresolved by the model.

2.1.4 Observation operators for reactive gases

The observations of chemically reactive gases that are assimilated into the IFS are satellite retrievals. These observations are total or partial column data, i.e. integrated layers bounded by a top and a bottom pressure. The unit for the reactive gases observations used in IFS is kg/m^2. The IFS background fields are interpolated in time and space to the location of the observation, and the model's first-guess is calculated as a simple vertical integral between the top and the bottom pressure given by the partial or total column.

It is also possible to use averaging kernels provided by the data producers in the observation operator. In this case, the model equivalent of the observation is calculated using the averaging kernel weights and pressures.

NO_2 - NOx interconversion The fast diurnal NO_2 - NO interconversion caused by solar radiation in the upper stratosphere can not be handled by the coupled system with a coupling frequency of one hour. Therefore NOx is used as the model variable instead of NO_2. The NOx field is not so strongly influenced by solar radiation and the chemical development of the NOx field can be simulated better by the coupled system. The use of NOx also reduces spatial variablity everywhere which is of advantage for the data assimilation. Since the satellite observations assimilated in the GEMS system are NO_2 data, a diagnostic NO_2/NOx interconversion operator was developed, including its tangent linear and adjoint. This operator is based on a simple photochemical equilibrium between NO_2 and NO:

$$\frac{[NO_2]}{[NOx]} = \frac{k[O_3]}{JNO2 + k[O_3]}. \tag{2}$$

Here k is the rate coefficient of the reaction of O_3 with NO to NO_2 and O_3 and depends on temperature, and JNO2 is the NO_2 photolysis frequency and depends on surface albedo, solar zenith angle, overhead ozone column, cloud optical properties and temperature. A parameterised approach for the calculation of JNO2 was used based on the band scheme by Landgraf and Crutzen (1998) in combination with actinic fluxes parameterised following Krol and Van Weele (1997). The diagnostic operator includes the effect of clouds, surface albedo and overhead ozone columns. Information for these fields is taken from the IFS. The parameterization was extended to include an adjustment to the equilibrium because of hydro-carbons in the lower troposphere and abundant O-radical in the higher stratosphere and mesosphere. An ad-hoc approach was introduced to account for the influence of per-oxy-radical concentration by assuming a per-oxy-radical (HO2 + RO2) concentration of 80 ppt (Kleinman et al. 1995) in the troposphere, which was scaled by the cosine of the solar zenith angle to account for the diurnal cycle of the per-oxy-radical concentration.

2.1.5 Bias correction and quality control for reactive gases

For the initial analysis experiments with the GEMS coupled system no bias correction is used for the reactive gases. This will be addressed in further studies.

Variational quality control and first-guess checks are applied to the reactive gases observations, apart from SO_2 observations.

2.2 Coupling and resolution

In the coupled setup the IFS and the CTM run in parallel, exchanging fields through the OASIS4 coupler every hour. This means the IFS supplies the meteorological data and updated mixing ratios for the GEMS species O_3, CO, NOx, HCHO, and SO_2 to the CTM every hour, and the CTM provides IFS with initial conditions for

the GEMS species and with chemical tendency fields every hour. These are tendencies due to chemistry, wet deposition and atmospheric emissions, and tendencies due to surface fluxes (emission, dry deposition). The tendencies are combined before the exchange and one total tendency is given from the CTM to the IFS.

The data assimilation algorithm for the GRG fields in the coupled system follows the assimilation of the IFS ozone with the parameterized chemistry (Hólm et al. 1999; Dethof and Hólm 2004). The implementation of the incremental solution for the 4D-VAR data assimilation problem is structured into an outer and inner loop. The outer loop, or trajectory run, is an IFS run with the complete model at high horizontal resolution to determine the increments between the model and the observations. The inner loop, or minimization run, is run with a linearized model version and its adjoint formulation at a lower resolution. The simplified model used in the inner loop acts on the increments to solve the minimization problem of the 4D-VAR cost function. The sequence of outer and inner loop is repeated two or more times to determine the final analysis. The time length of the assimilation window is 12 hours, and analyses valid every 6 hours are produced. A forecast run started from the previous analysis provides the starting point for the assimilation in the next 12h window.

The IFS-CTM coupling is applied in the outer loops. The inner loops using the tangent linear and adjoint model are currently run uncoupled, i.e. without the application of the source and sink tendencies from the CTM. The subsequent forecast that provides the starting point for the next analysis cycle is run coupled.

In the coupled system the IFS runs at a T159 spectral resolution and the grid point space is represented in a reduced Gaussian grid (Hortal and Simmons 1991). The vertical coordinate system is given by 60 hybrid sigma-pressure levels, with a model top at 0.1 hPa. In order to avoid difficulties in the vertical interpolation by the OASIS4 coupler, the CTMs use the same 60 vertical levels. The coupler only has to perform horizontal interpolations for which the bi-linear mode is applied. The resolution of the CTMs is between 2° and 3°, lower than the IFS resolution, because of the high computational cost of the CTMs. The IFS is run on a higher horizontal resolution because of the quality of the meteorological forecasts and because a lower resolution would limit the acceptance of high resolution observations within data assimilation. The coupling frequency is 3600 s which is the largest acceptable time step for the IFS at a T159 resolution. More details of the CTMs and the coupling setup are given in Flemming et al. (2009).

3 Results

This section presents some results of the assimilation of O_3, CO, NOx, HCHO and SO_2 obtained with the coupled GEMS assimilation system. Data for the assimilation of O_3 and CO are taken from a GRG reanalysis run for the period May to December 2003 (GRGAN), in which the MOZART CTM was coupled to the IFS and GRG data were assimilated in addition to the meteorological data assimilated at ECMWF during 2003. These GRG data include MOPITT total column CO data, total column O_3 data from SCIAMACHY, and partial O_3 columns from MIPAS, GOME and SBUV/2. In addition to GRGAN, a control experiment was run, in which the GRG data were only included passively (GRGCTRL). A comprehensive evaluation of GRGAN and GRGCTRL is done elsewhere (e.g. Ordonez et al. 2009; Elguindi et al. 2009; GEMS GRG validation report 2009). Here only some examples for O_3 and CO are shown.

NO_2 and HCHO data were not assimilated in GRGAN, because the technical development for the assimilation of those fields had not been completed. SO_2 was not included in the version of the MOZART model that was used for these coupled runs. The examples for the assimilation of NO_2, HCHO and SO_2 that are shown here are taken from other assimilation experiments.

3.1 GEMS O_3 assimilation

The ozone retrievals assimilated in GRGAN are total column ozone fields from SCIAMACHY produced by KNMI, GOME ozone profiles produced by the Rutherford Appleton Laboratory, MIPAS ozone profiles produced by ESA, and SBUV/2 partial columns from NOAA. Because MIPAS measures in the mid-infrared part of the spectrum, MIPAS ozone data are the only data used here that are available independent of illumination condition, including during the polar night. The SCIAMACHY data are thinned to a horizontal resolution of 0.5°x0.5°, the other ozone data are not thinned. SCIAMACHY, GOME and SBUV/2 ozone data are not used at low solar elevations, and GOME and SBUV/2 data are not used poleward of 80°. Profile data are not assimilated above 1 hPa.

Figure 5 shows timeseries of zonal mean total column ozone from GRGAN, GRGCTRL and independent TOMS data for the period 1 May to 31 December 2003. The total column timeseries from GRGAN agrees well with the independent TOMS data. It shows high values at high northern latitudes and in SH midlatitudes, lower values in the tropics, and the very low values of the Antarctic Ozone hole between September and November. The control experiment agrees less well with the TOMS data. It underestimates total column ozone in the Tropics, and overestimates it in SH midlatitudes. The Antarctic ozone hole is not deep enough in GRGCTRL, and zonal mean ozone values are 100 Dobson Units higher in GRGCTRL than in GRGAN at the peak of the ozone hole. This overestimation of the ozone column in the SH was also found in standalone runs with the MOZART CTM (GEMS GRG validation report 2009).

Figure 6 depicts seasonal mean plots of total column ozone for June to August (JJA) and September to November (SON) 2003 (left panels) from GRGAN, and the difference between GRGAN and GRGCTRL (right panels). It shows that the assimilation leads to reduced ozone columns in the NH extratropics and to increased values in the tropics in both seasons in GRGAN. The control run overestimates the stratospheric ozone maximum in the NH extratropics and underestimates it in the tropics, and the assimilation corrects this. This leads to the improved agreement with TOMS data seen in Figure 5. In SH midlatitudes and over the South Pole the control run overestimates the ozone columns, and the assimilation leads to reduced total column ozone values in GRGAN.

The largest change in total ozone column between GRGAN and GRGCTRL is seen over the South Pole where the ozone hole is not deep enough in GRGCTRL (Figures 5 and 6). Figure 7 takes a closer look at the ozone field over the South Pole on 4 October 2003. It shows a cross section of ozone across the South pole along 8°E from GRGAN (top), GRGCTRL (middle), as well as ozone profiles from an independent ozone sonde launched at Neumayer (71°S, 8°E) and from GRGAN and GRGCTRL. Both, the cross sections and the ozone profiles, illustrate that the depletion of ozone over the South Pole in the layer between 25-150 hPa is completely missing in the control run, while GRGAN shows low ozone values over the pole and agrees well with the ozone sonde observation.

The examples shown here illustrate that the assimilation of ozone data in the GEMS coupled system leads to an improved total column ozone field in comparison with the control run. The analysis also improves the vertical structure of the GEMS ozone field if ozone profile data, such as MIPAS or GOME profiles, are assimilated. Total column and profiles from GRGAN agree well with independent observations from TOMS and ozone sondes.

3.2 CO assimilation

Total column CO retrievals from MOPITT version 003 (Deeter et al. 2003) are assimilated in GRGAN. The data are thinned to a resolution of 0.5°x0.5° and are only assimilated over land between 65°N and 65°S. Averaging

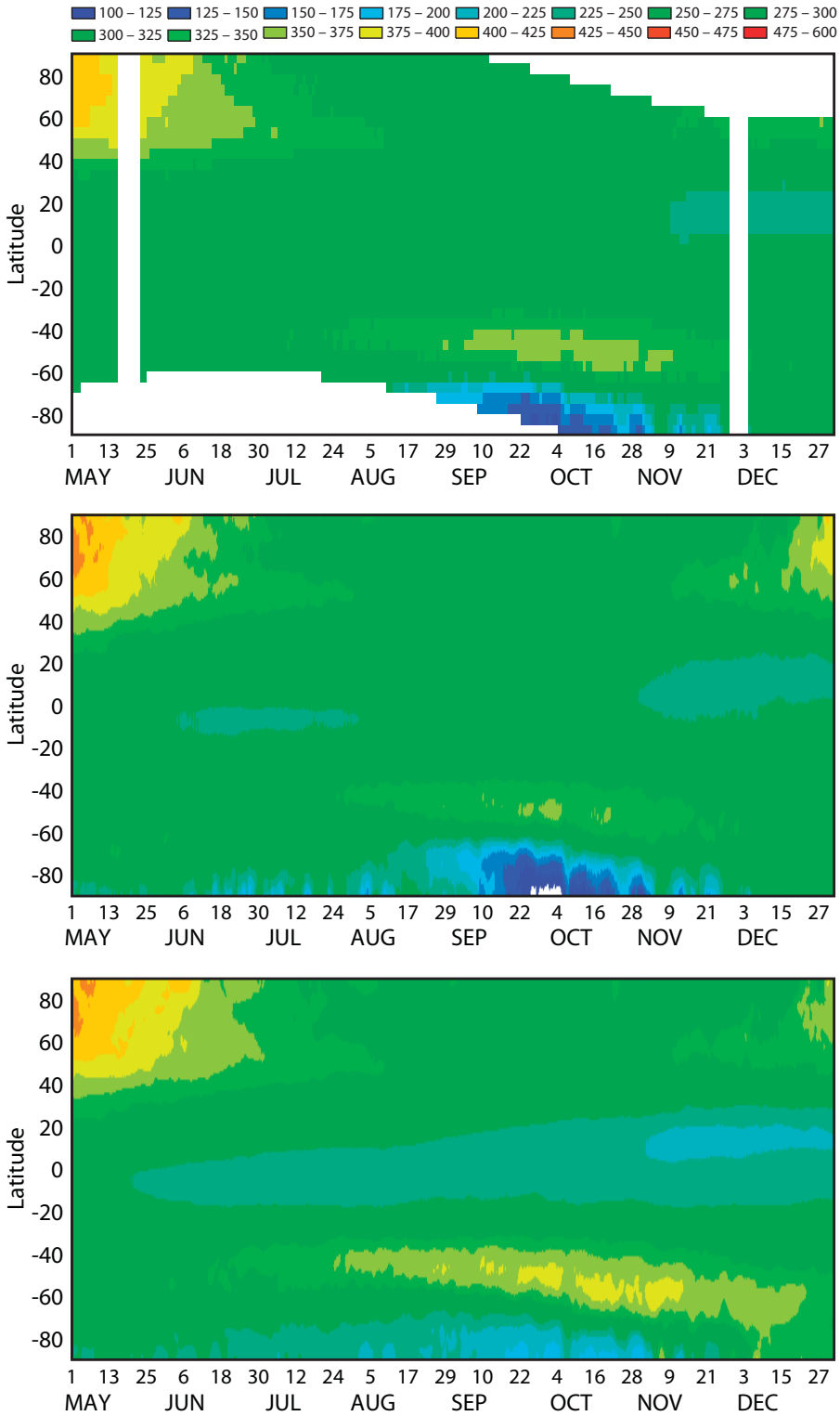

Figure 5: Timeseries of zonal mean total column ozone in Dobson Units for the period 1 May 2003 till 31 December 2003 from TOMS data (top), GRGAN (middle) and GRGCTRL (bottom).

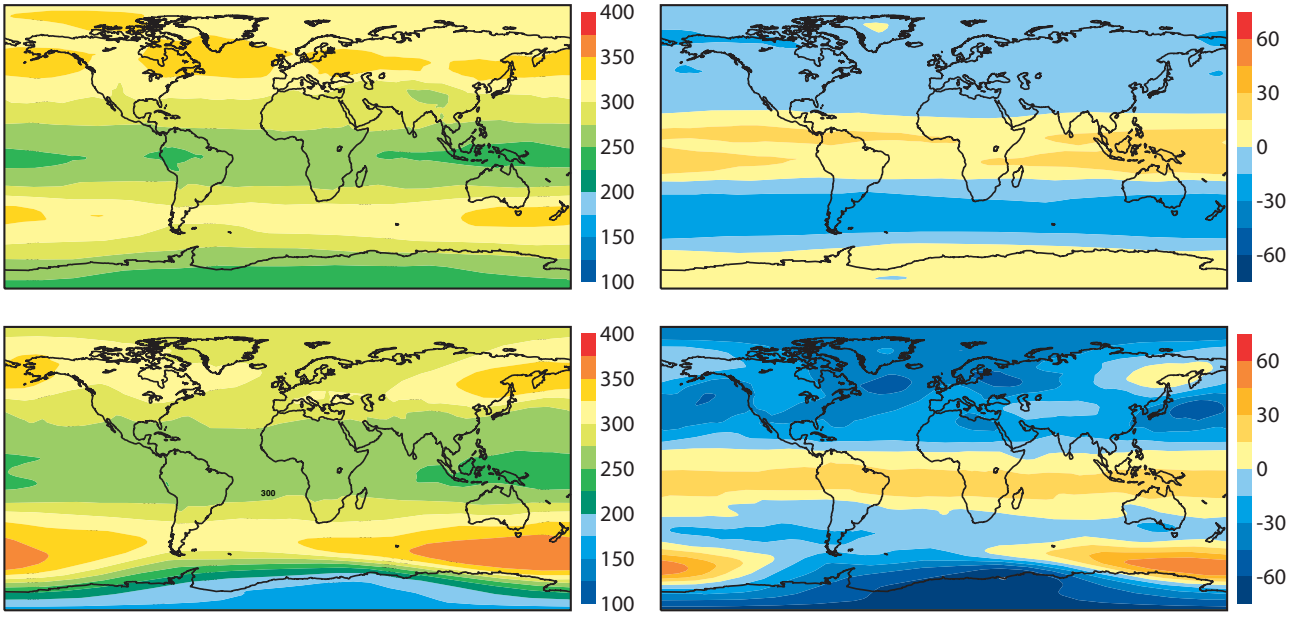

Figure 6: Mean total column GEMS ozone field in Dobson Units averaged over the seasons JJA (top) and SON (bottom). The left panels show GRGAN, the right panels the difference between GRGAN and GRGCTRL (GRGAN minus GRGCTRL) also in Dobson Units.

kernel information from the MOPITT data is not used in the experiments presented here.

Figure 8 shows a timeseries of globally averaged CO total column first-guess and analysis departures and their standard deviations, as well as the number of observations used per analysis cycle between May and December 2003. Plotted are statistics for data that are actively used in the analysis. The timeseries shows that the assimilation is working well and that the analysis is drawing to the data. The biases (dotted lines) are reduced by the analysis, and after an initial spin-up in May the bias is close to zero. The standard deviations of the departures are also reduced. The standard deviation of the analysis departures is about 10% of the global mean total column CO values from GRGAN which lie between 1.7 and 1.8×10^{18} mol/cm^2.

Figure 9 shows the seasonal mean total column CO fields for JJA and SON 2003 from GRGAN (left panels) and the difference between GRGAN and GRGCTRL (right panels). GRGAN shows realistic total column CO values. During both seasons values are higher in the NH than in the SH. CO maxima are found over tropical Africa and South America in both seasons, as well as over North America and Eastern Siberia during JJA and over China during SON. During JJA the assimilation increases the CO values in the NH midlatitudes and reduces total column CO in the tropics and SH. During SON, the assimilation leads to increased total column values compared to the control run over the biomass burning areas in tropical Africa and South America. The total column over the tropical Pacific is reduced in GRGAN. Again CO column values in NH midlatitudes are increased and values are reduced over much of the equatorial tropics.

To compare the analyzed CO field with independent data that are not used in the analysis, CO profiles from GRGAN and GRGCTRL are compared with CO profiles from the MOZAIC (Measurement of Ozone, Water Vapour, Carbon Monoxide and Nitrogen Oxides by Airbus in-service Aircraft) programme (Nedelec et al. 2003). Figure 10 shows monthly mean CO profiles for September to November 2003 over Frankfurt and Osaka from GRGAN, GRGCTRL and MOZAIC data. The MOZAIC profiles were taken during aircraft ascents and descents at Frankfurt and Osaka airport. The assimilation of MOPITT CO data improves the fit to the MOZAIC data in GRGAN compared to GRGCTRL over both airports. However, both GRGCTRL and GRGAN underestimate the CO concentrations in the lower troposphere, particularly near the surface. It is possible that this

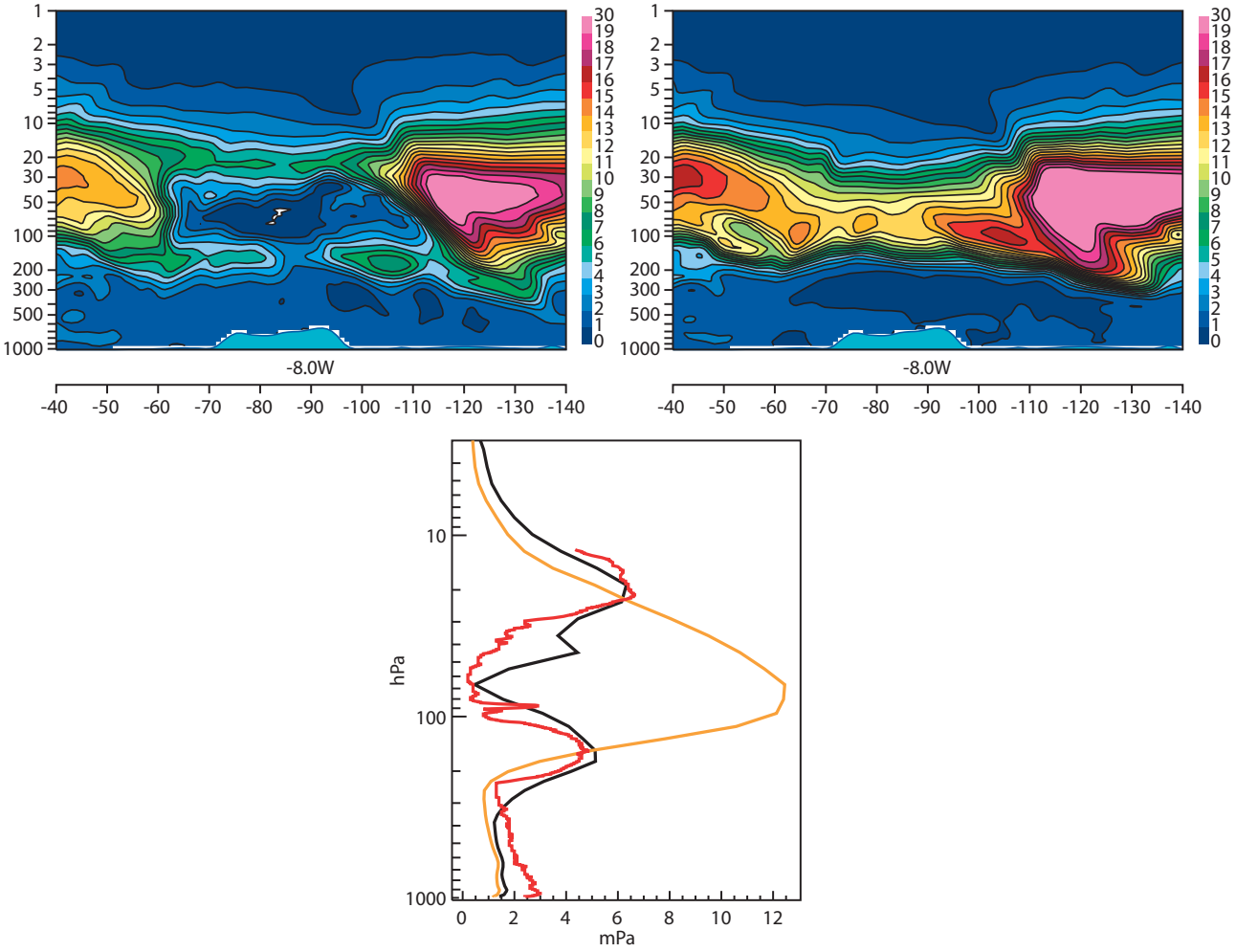

Figure 7: Ozone cross section from 40°S across the South Pole back to 40°S along 8°E from GRGAN (top left) and GRGCTRL (top right) on 4 October 2003, 12z. The bottom panel shows ozone profiles at the Neumayer station (71°S, 8°E) from an ozone sonde launched on 4 October 2003 (red), GRGAN (black) and GRGCTRL (orange). The Unit is mPa.

is a representativeness error and the model with a horizontal resolution of T159 (corresponding to a reduced Gaussian grid of about 125 km x 125 km) is not able to reproduce the high values observed by MOZAIC over both airports. Alternatively, it could be a sign that the surface CO emissions used by the MOZART CTM are too low to reproduce the high CO values observed by MOZAIC in the lower troposphere.

3.3 NO_2 assimilation

To test the assimilation of NO_2 data with the coupled GEMS system, first a single observation experiment is carried out. For a single total column observation the shape of the analysis increment is given by BH^t. For diagonal B and R matrices this gives

$$H(x_a - x_b) = HBH^t(HBH^t + R)^{-1}(y - Hx_b) = \sigma_b^2\left(\frac{y - Hx_b}{\sigma_b^2 + \sigma_o^2}\right), \tag{3}$$

where x_a is the analysis value, x_b the background value, y the observation, H is the observation operator, B the background error covariance matrix, R the observation error covariance matrix, σ_b^2 the observation equivalent

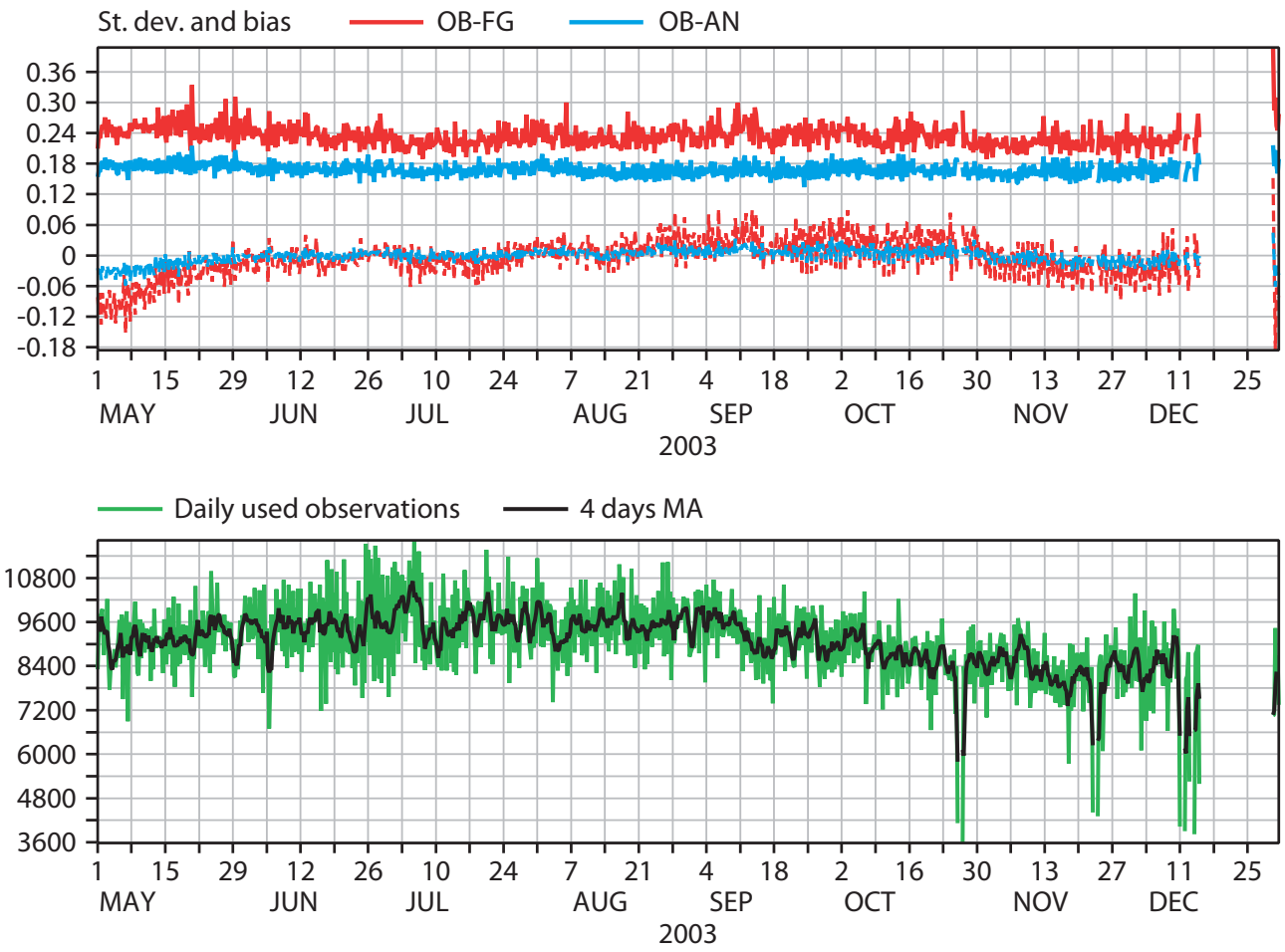

Figure 8: Timeseries of globally averaged MOPITT total column CO first-guess departures (red dotted line) and analysis departures (blue dotted line), as well as standard deviations of first-guess departures (red solid line) and of analysis departures (blue solid line) in 10^{18}mol/cm^2 (top panel), and number of observations per assimilation cycle (bottom panel) from GRGAN for used data.

of the background covariance and σ_o^2 the observation variance.

To investigate how the increment from one NO_2 observation is spread out in the vertical and horizontal, a single tropospheric column NO_2 observation is placed at 38.6°N, 119.3°E on 2 January 2006, 02:32:20 hours. The observation has a value of 28.8x10^{15} mol/cm^2 and an error of 20%. It is 19.1x10^{15} mol/cm^2 higher than the background. Averaging kernels for the observation are used in the observation operator. No variational quality control and first-guess checks are applied.

Figure 11 (top left panel) shows the total column NOx increment resulting from the assimilation of this observation. The NOx increment has a maximum value of 16.3x10^{15} mol/cm^2 at the location of the observation. The first-guess NO_2 value at the location of the observation is 9.7x10^{15} mol/cm^2 and the analysis NO_2 value 14.1x10^{15} mol/cm^2.

The top right panel of Figure 11 shows a vertical cross section through the analysis increment along 119.3°E. The impact of the observation is confined to the lowest five model levels. The absolute impact is largest around model level 57. The bottom panel of Figure 11 shows the vertical NOx analysis and first-guess profiles at the location of the observation and illustrates again how the analysis increment is distributed in the vertical.

A 1-month long NO_2 assimilation experiment (NO2AN) is run with the coupled GEMS system for January

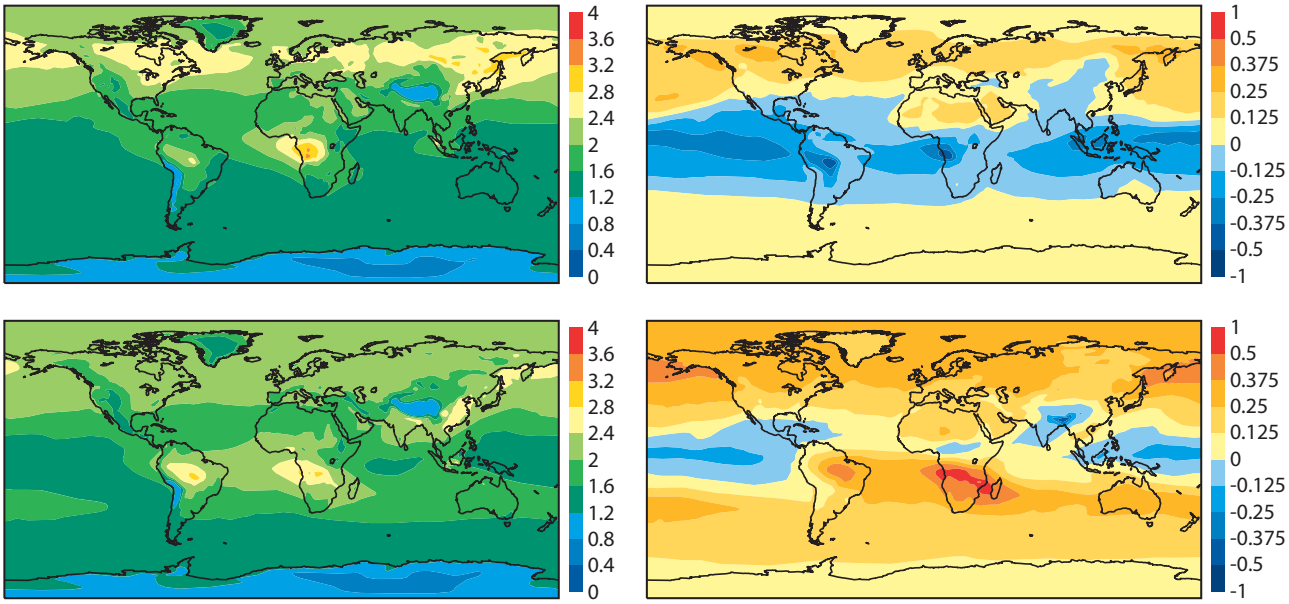

Figure 9: Mean total column CO field averaged over the seasons JJA (top) and SON (bottom) 2003. The left panels show GRGAN, the right panels the difference between GRGAN and GRGCTRL (GRGAN minus GRGCTRL). Unit is 10^{18} molecules/cm^2.

2006. The NO_2 data used in the assimilation experiment are tropospheric NO_2 columns from SCIAMACHY, derived by KNMI with a DOAS algorithm (http://www.gse-promote.org). The retrieval method and an error analysis of the retrieval are given in Boersma et al. (2004). The data have large errors in clean areas, dominated by errors in the spectral fitting and stratospheric column estimate. Over continental areas the error is of the order 35-60%. Best results are obtained in regions with strong NO_2 sources or high surface albedo. Areas with tropospheric column values greater than 1.0×10^{15} mol/cm^2 have errors of less than 50%. The data producers provide averaging kernels with the data, and this information is used in the observation operator for the assimilation. In addition to NO2AN a control experiment is run in which the SCIAMACHY NO_2 data are only included passively (NO2CTRL).

Figure 12 shows monthly mean tropospheric NOx columns (integral between model levels 35 and 60) from NO2AN for January 2006, the difference between the monthly mean tropospheric NO_2 column from NO2AN and NO2CTRL, as well as monthly mean tropospheric NO_2 values from OMI (note the different colour scales). The OMI data are independent data that were not used in the analysis. The analysis gives a realistic NOx field with high NOx values over North America, Europe, India and South-East Asia. It also shows up biomass burning areas in tropical Africa and elevated NOx values over several cities in the SH. The control run has higher NOx concentrations almost everywhere, with the exception of some biomass burning areas in Africa, and some pollution hot spots over Beijing, and several Indian cities.

Figure 13 shows a timeseries of globally averaged NO_2 tropospheric column first-guess and analysis departures from NO2AN and their standard deviations, as well as the number of observations per analysis cycle. Plotted are statistics for data that are actively used in the analysis in January 2006. The timeseries shows that the analysis is drawing to the data, and that departures and their standard deviations are reduced. However, a small bias (dotted lines) remains in the analysis, and the differences between the standard deviations of the first-guess and analysis departures are not as large as the ones seen for the CO assimilation (Figure8). This suggests that either the background errors for NOx are too tight, or that because of the larger observation errors of the NO_2 data a smaller correction is carried out by the analysis.

The spikes seen in Figure 13 on 8, 11, 15, and 27 January, 0z, are due to high observed NO_2 values over

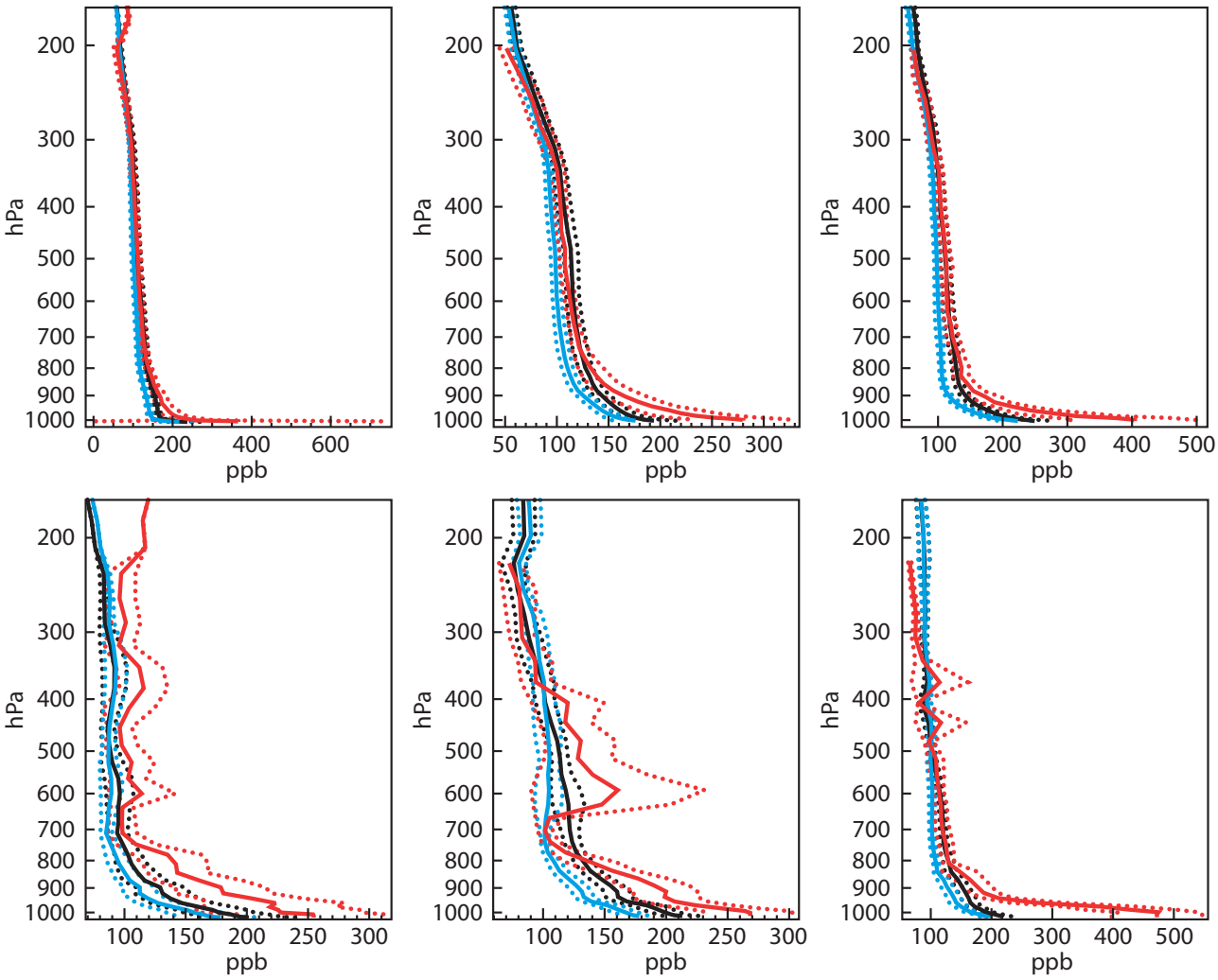

Figure 10: Monthly mean CO profiles over Frankfurt (top panels) and Osaka (bottom panels) from GRGAN (black), GRGCTRL (blue) and independent MOZAIC data (red) for September (left panels), October (middle panels), and November 2003 (right panels) in ppb. The solid lines show the mean profiles, the dotted lines +/- one standard deviation.

South East Asia. An example is given in Figure 14 that shows the analyzed tropospheric NOx column from NO2AN and NO2CTRL on 20060111, 0z, their difference (NO2AN minus NO2CTRL), and the tropospheric NO_2 columns from SCIAMACHY that were used in the analysis. The observations show high NO_2 values over China, Japan and North-East India, and the analysis reproduces these high values well. The control run has lower NOx concentrations over the polluted areas than the analysis, but higher background concentrations.

The examples shown here indicate that the NO_2 analysis is working well. A more detailed validation study will have to be carried out, including a thorough comparison with independent NO_2 observations.

3.4 HCHO assimilation

To test the assimilation of HCHO data with the coupled GEMS system, first a single observation experiment is carried out. A single total column HCHO observation is placed at 49.4°N, 136.4°E on 1 July 2006, 01:31:18 hours. The observation has a value of 30×10^{15} mol/cm^2 and an error of 20%. It is 15.7×10^{15} mol/cm^2 higher than the background. Averaging kernels for the observation are used in the observation operator. No variational

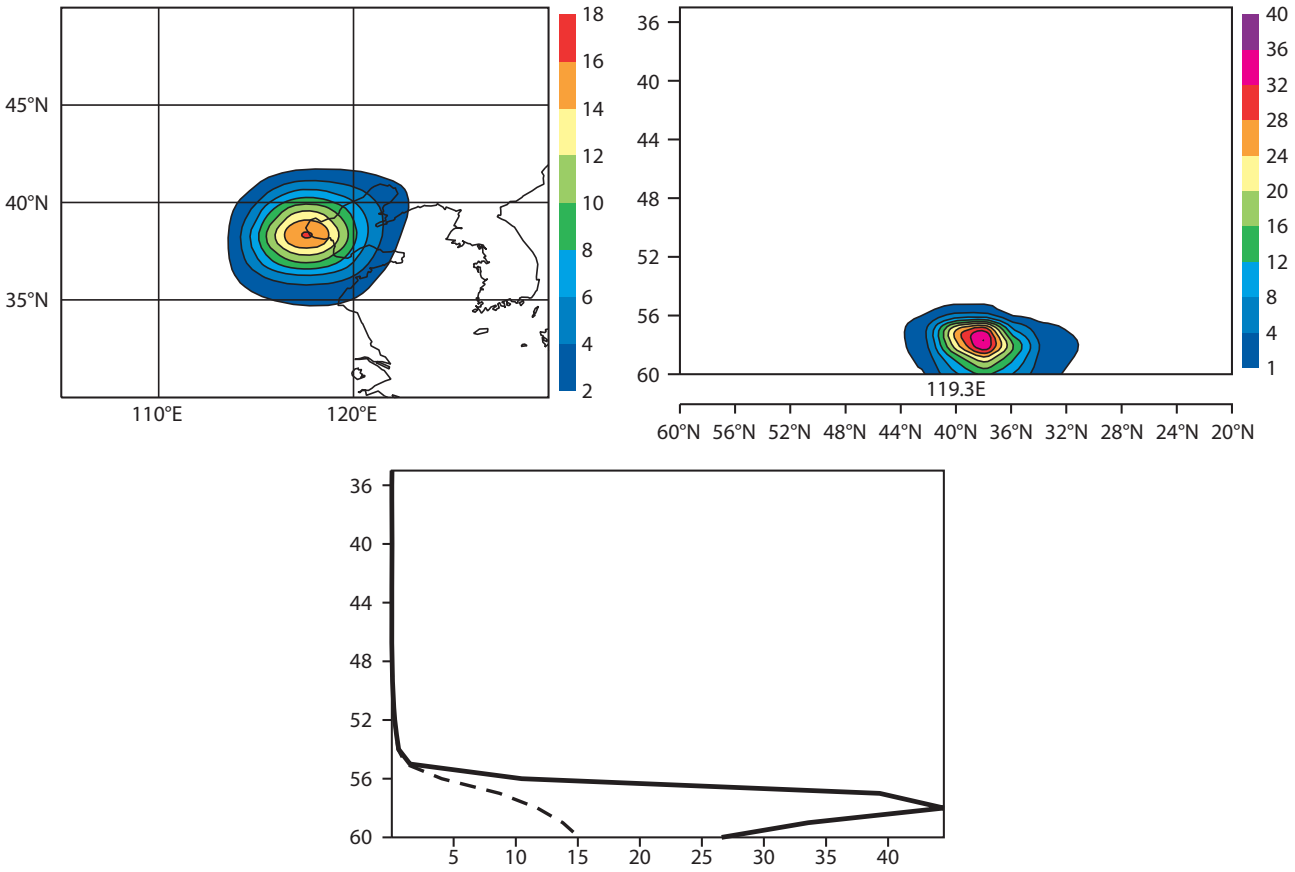

Figure 11: Tropospheric column (integral between model levels 35 and 60) NOx analysis increment (top left) in 10^{15}mol/cm^2, vertical cross section of analysis increment at 119.3°E in ppb (top right), and NOx analysis (solid) and first-guess (dashed) profiles in ppb (bottom) from a single NO_2 tropospheric column observation placed at 38.6°N, 119.3°E on 20060102, at 02:32:20 hours.

quality control and first-guess checks are applied. Figure 15 (top left panel) shows the total column increment resulting from the assimilation of this observation. The increment has a maximum value of 4.4x10^{15} mol/cm^2 at the location of the observation. The first-guess value at the location of the observation is 14.3x10^{15} mol/cm^2 the analysis value is 18.7x10^{15} mol/cm^2. The magnitude of the increment agrees with what is expected from theoretical arguments (Equation 3).

The top right panel of Figure 15 shows a vertical cross section through the analysis increment along 136.4°E. The absolute impact of the observation is largest around model level 55. However the impact of the observation can be seen throughout the troposphere (up to level 30). The bottom panel of Figure 15 shows the vertical HCHO analysis and first-guess profiles at the location of the observation and illustrates again how the analysis increment is distributed in the vertical.

A 1-month long HCHO assimilation experiment (HCHOAN) is run with the coupled GEMS system for August 2008. The HCHO data used in HCHOAN are total column HCHO data produced by the Belgian Institute for Space Aeronomy (BIRA) for the PROMOTE project (http://www.gse-promote.org). Information about the retrieval and the data quality can be found in De Smedt et al. (2006). Monthly mean HCHO values have total errors of 20-40%, individual pixels have much larger total errors, dominated by the random error. Because the total error of the data increases with latitude, only data between 50°N and 50°S are used in GRGAN. Data with a cloud fraction greater than 40% are also rejected, and no data are used over the area of the South Atlantic Anomaly. The data producers provide averaging kernels with the data, and this information is used in the

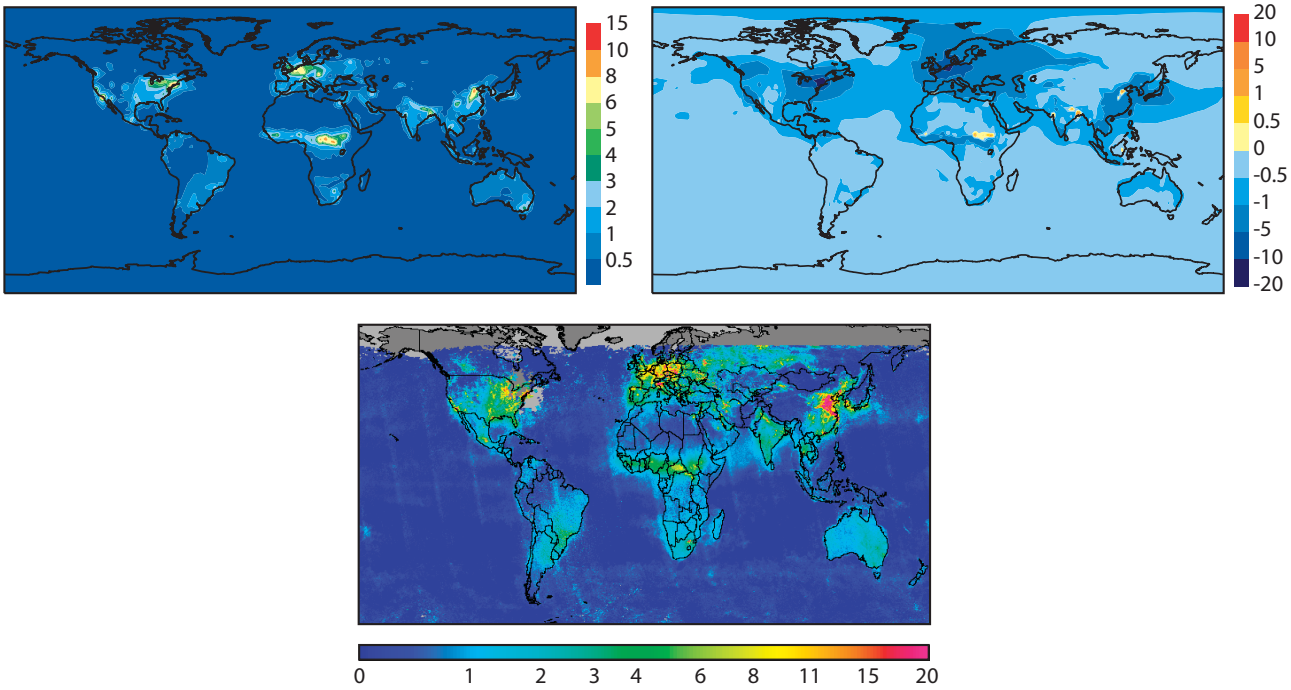

Figure 12: Tropospheric NOx columns (integral between model levels 35 and 60) from NO2AN (top left), difference between NO2AN and NO2CTRL (top right), and monthly mean tropospheric NO_2 from OMI (bottom panel). Unit is 10^{15}mol/cm^2. The OMI plot was taken from http://www.gse-promote.org/.

observation operator for the assimilation. Because of the noise in the data, it is not ideal to use the data for an assimilation experiment. They would be better suited to monthly mean validation studies. However, because no other HCHO data are available, the data are used in HCHOAN despite their shortcomings.

Figure 16 shows a timeseries of globally averaged HCHO tropospheric column first-guess and analysis departures and their standard deviations for August 2007, as well as the number of observations used per analysis cycle. Plotted are statistics for data that are actively used in the analysis. The timeseries shows that the analysis is drawing to the data and that bias and standard deviation of the departures are reduced. However, a considerable bias remains and the standard deviation of the analysis departures remains large, indicating that there is a lot of noise in the data.

Figure 17 shows the monthly mean total column HCHO field from HCHOAN for August 2007, the monthly mean difference between HCHOAN and HCHOCTRL and the monthly mean total column HCHO field from independent OMI data (note the different colour scales). The analysis produces a realistic looking total column HCHO field that agrees well with the independent OMI data. The assimilation leads to increased HCHO values over the oceans and reduced values over land.

These first results show that the assimilation of HCHO data with the coupled GEMS system is working in principle. However, better quality data are needed if HCHO data are to be assimilated in longer reanalysis runs with the GEMS system.

3.5 SO_2 assimilation

The coupled system will only be used to assimilate SO_2 observations for case studies of volcanic eruptions. As an example, the eruption of Mount Nyamuragira in central Africa in 2006 is presented here. Nyamuragira began

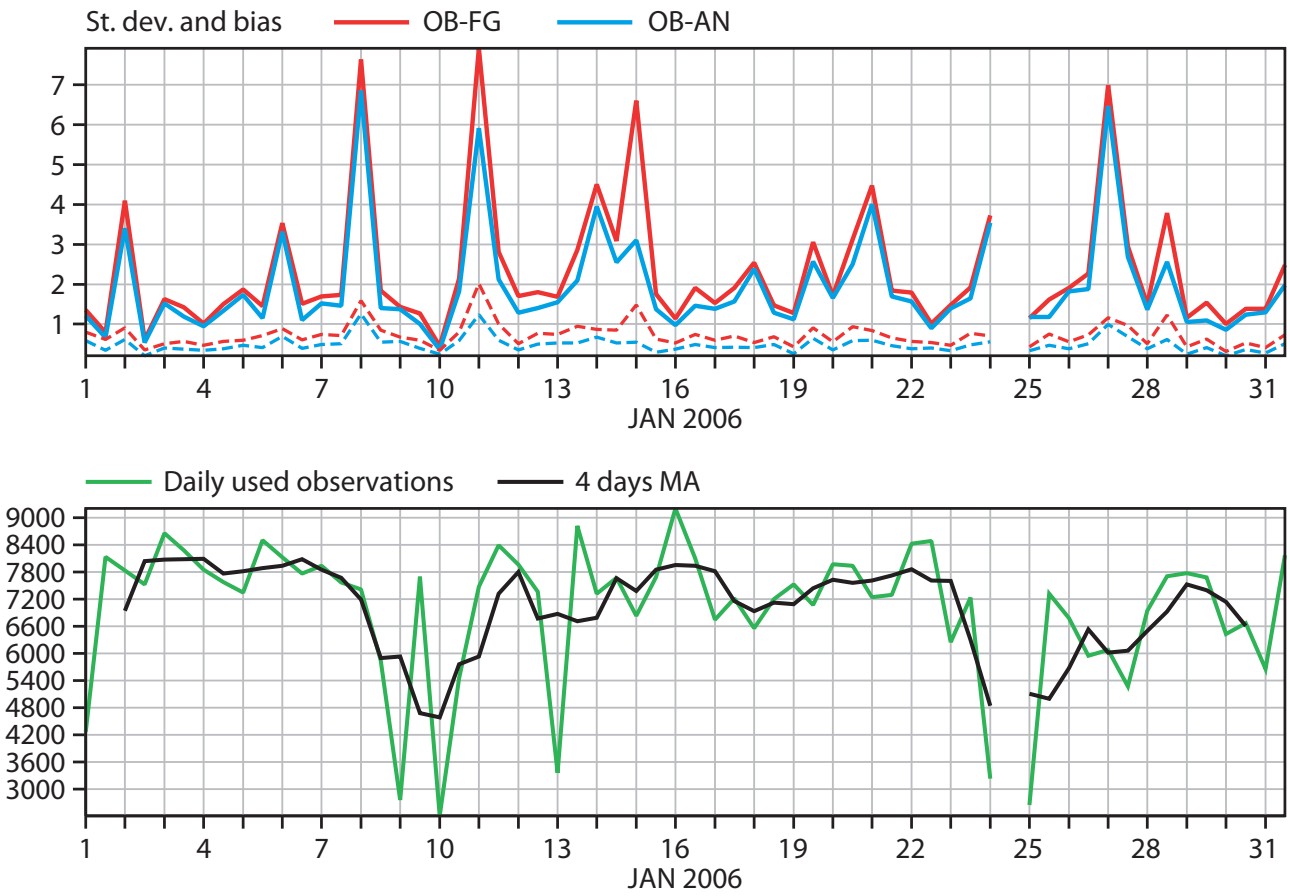

Figure 13: Timeseries of globally averaged SCIAMACHY tropospheric column NO_2 first-guess departures (red dotted line) and analysis departures (blue dotted line), as well as standard deviations of first-guess departures (red solid line) and analysis departures (blue solid line) in 10^{15}mol/cm^2 (top panel), and number of observations per assimilation cycle (bottom panel) from NO2AN for used data for January 2006.

erupting on 27 November 2006 around 10pm local time, and SO_2 emissions were observed by the OMI instrument until 4 December (see http://so2.umbc.edu/omi/ and http://earthobservatory.nasa.gov/IOTD/view.php?id=7189.). The OMI observations show that the SO_2 plume first travelled westward, then moved in a clockwise direction towards the northeast, and eventually reached India (see Figure 18).

For the SO_2 assimilation experiment of the Nyamuragira eruption (SO2AN) total column SO_2 retrievals from SCIAMACHY are used that were produced by BIRA for the PROMOTE project (http://www.gse-promote.org). Information about the retrieval and the data quality can be found on the PROMOTE website. BIRA produce three different vertical column density retrievals, for three different assumed plume heights (1 km above ground, 6 km, and 14 km). Here, the BIRA retrieval that assumes a plume height of 6km is used, and a SO_2 JB that peaks at 6 km (see Figure 4) for first assimilation tests. Unfortunately, no SCIAMACHY data are available over Africa between 28-30 November, so that SO2AN is only started on 1 December, 0z, three days after the volcanic eruption began. SO_2 data are only assimilated in the area between 30°N and 30°S, 0° and 40°E and blacklisted elsewhere.

Figure 19 shows maps of total column SO_2 in Dobson Units from SO2AN. The background forecast (top left) shows elevated SO_2 concentrations over North America, Europe, Russia, India and China. The background forecast does not show any elevated SO_2 values over Africa, because the MOZART CTM that provides the initial SO_2 field does not know about the Nyamuragira eruption. By assimilating the SCIAMACHY SO_2 data

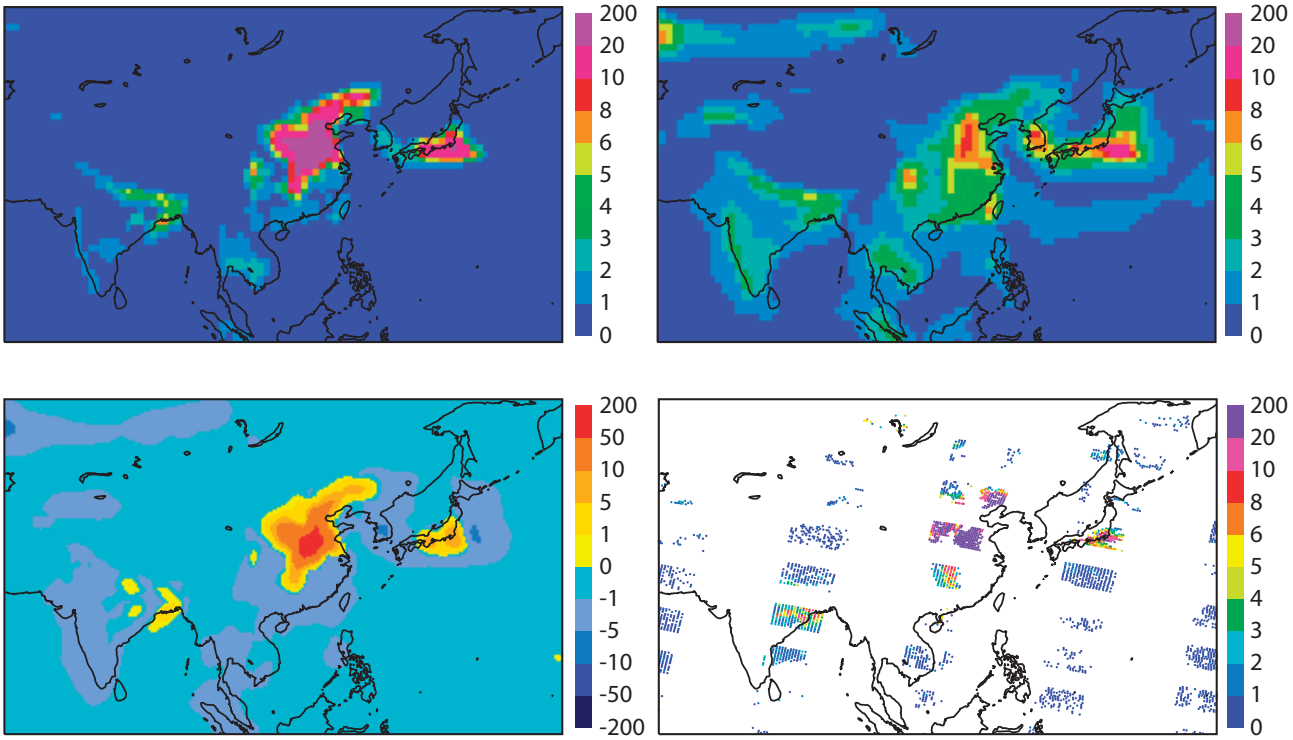

Figure 14: Tropospheric NOx columns (integral between model levels 35 and 60) from NO2AN (top left), NO2CTRL (top right), difference between NO2AN and NO2CTRL (bottom left), and SCIAMACHY tropospheric NO_2 columns (bottom right) that were used in the assimilation on 20060111, 0z. Unit is $10^{15} mol/cm^2$.

(Figure 19 top right panel) this information is brought into the analysis (middle left). The plume then spreads north westwards and eventually eastwards in the NH and to a lesser extent into the SH. It reaches India and Australia by 3 December (bottom left), and NH central Pacific by 6 December (bottom right). Our analysis values are lower than the values observed by OMI (see Figure 18), but on the whole our SO_2 analysis patterns agree well with the OMI observations (Figure 18). The maximum values of the assimilated SCIAMACHY SO_2 data are lower than those of the OMI data, probably because of the larger pixel sizes and bigger data gaps of SCIAMACHY.

Figure 20 shows area averaged SO2 profiles from SO2AN for an area over Africa (left panel) and a clean area over the north-west Pacific (right panel) on 1, 3, and 6 December 2006. The Africa profiles show large SO_2 values in the middle troposphere where the assimilation places the bulk of the volcanic SO_2. It also shows how the SO_2 concentrations spread out in the vertical with time, as SO_2 is transported by the model. SO_2 concentrations decrease after the eruption between 3 and 6 December, but even on 6 December maximum values are still greater than 10 ppb. The profiles over the clean area over the north-west Pacific show an increase in SO_2 concentrations on 3 and 6 December, because SO_2 from the volcanic eruption has been transported here. Overall the SO_2 concentrations in the clean area are a factor of 10 lower on 6 December than over Africa.

These first results from the assimilation of SO_2 data are encouraging. The coupled system manages to reproduce realistic SO_2 patterns if SCIAMACHY SO_2 data are assimilated, even if there are no volcanic emissions in the background model. It has to be kept in mind that the vertical structure of the analyzed SO_2 field entirely depends on the background error covariances, which in this case prescribe an injection height of 6km. The case study will be repeated when OMI SO_2 data are available for that period, because OMI has a better data coverage and also provides data for the first three days after the eruption.

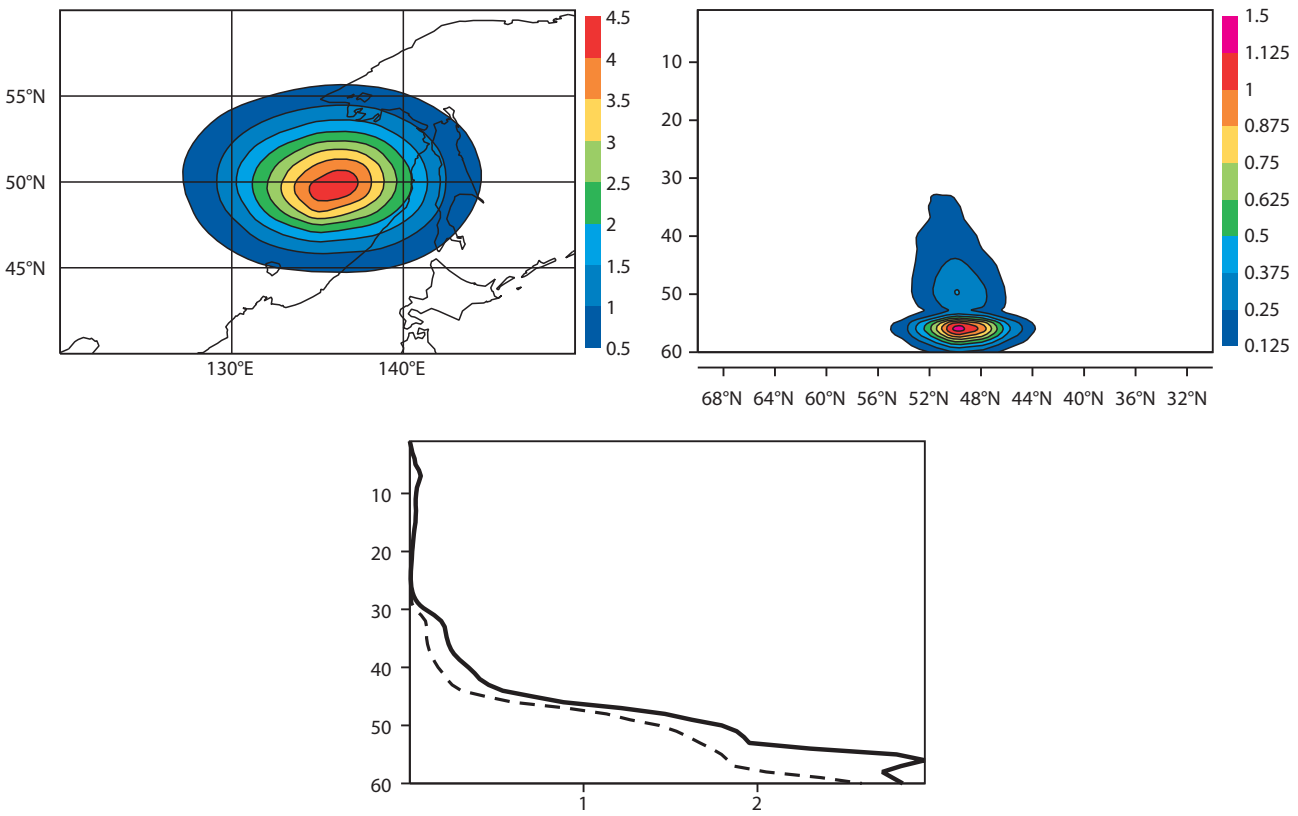

Figure 15: Total column HCHO analysis increment (top left) in 10^{15}mol/cm^2, vertical cross section of analysis increment at 136.4° E in ppb (top right), and HCHO analysis (solid) and first-guess (dashed) profiles in ppb (bottom) from a single HCHO observation placed at 49.4° N, 136.4° E on 20060701, at 01:31:18 hours. The observation has a value of 30x10^{15} mol/cm^2 and an error of 20%, and is 15.7x10^{15} mol/cm^2 higher than the background.

4 Conclusions and outlook

A data assimilation system for the chemically reactive gases O_3, CO, NOx, HCHO, and SO_2 has been developed as part of the EU funded GEMS project, by coupling the three CTMs MOZART, MOCAGE and TM5 to ECMWF's IFS using the OASIS4 coupler. In this paper, the GEMS GRG assimilation system was described and some first results were shown that were obtained with the coupled system where the MOZART CTM was coupled to IFS. The background error statistics for O3 were obtained with the analysis ensemble method, the background error statistics for CO, NOx and HCHO were based on the NMC method. Background errors for SO_2 were prescribed to mimic the deposit of volcanic SO_2 in the free troposphere. Assimilation experiments were carried out for all five species, assimilating O3 retrievals from SCIAMACHY, MIPAS, GOME and SBUV, CO retrievals from MOPITT, and NO2, HCHO and SO2 retrievals from SCIAMACHY. Results from these assimilation experiments illustrate that the coupled approach is working successfully and that the reactive gases assimilation system gives realistically looking results.

It is planned to carry out more comprehensive validation studies against independent observations for assimilation experiments of all five species and to present these in future studies. Further effort will also be spent on improving the coupled system. The CTMs are constantly improved, and these improvements will be included in the coupled system. Aspects of the data assimilation system will also be refined. For example, it is planned to recalculate the background error statistics for the reactive gases with the NMC method using a newer version of the coupled system, and in the longer term the analysis ensemble method will be used to calculate new statistics

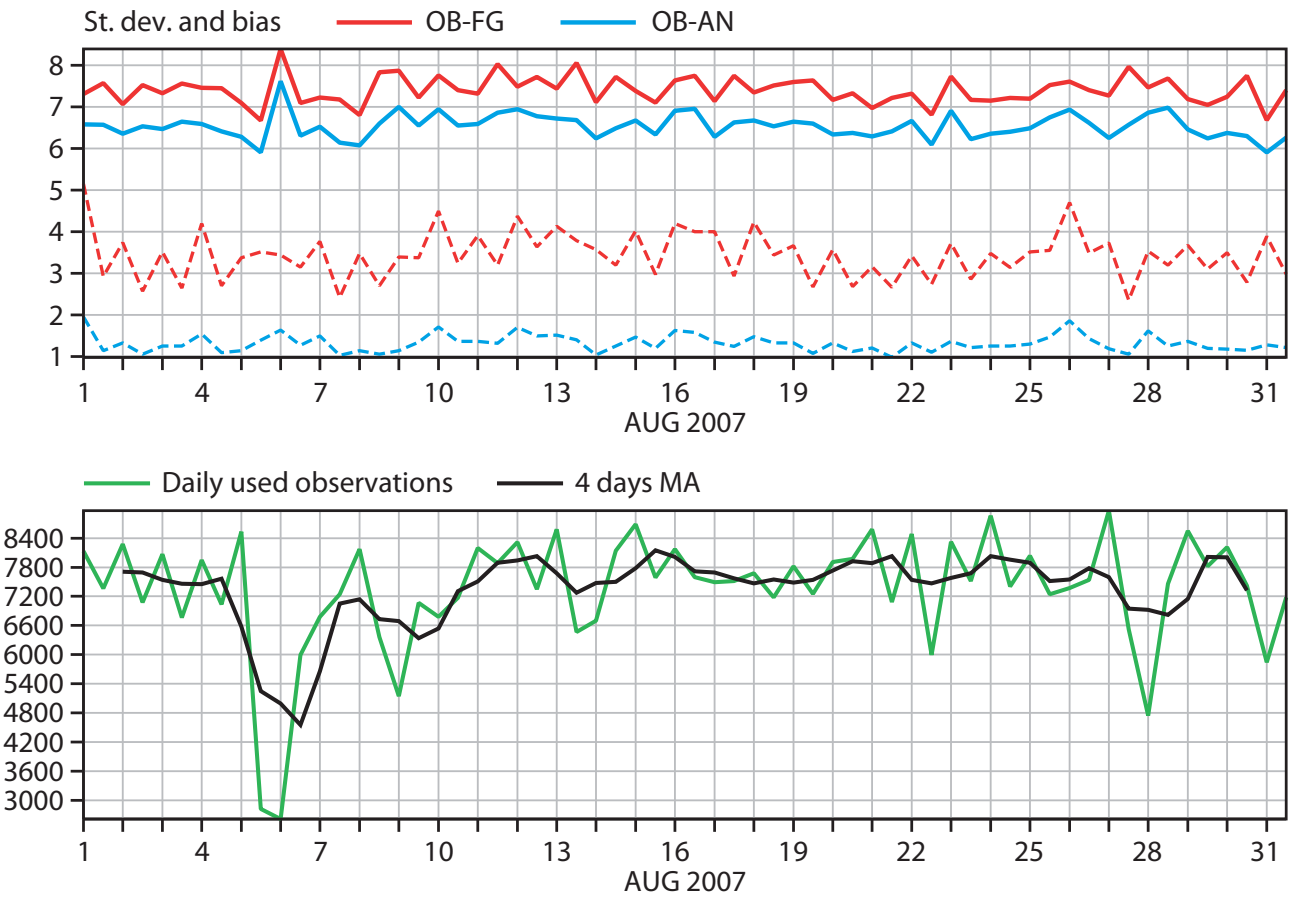

Figure 16: Timeseries of global mean SCIAMACHY tropospheric column HCHO first-guess departures (red dotted line) and analysis departures (blue dotted line), as well as standard deviations of first-guess departures (red solid line) and analysis departures (blue solid line) in 10^{15}mol/cm^2 (top panel), and number of observations per assimilation cycle (bottom panel) from HCHOAN for used data for August 2007.

for the GRG fields. A bias correction scheme is being developed for the GRG fields and will be used in future studies.

The coupled assimilation system was used in collaboration with the greenhouse gas and aerosol subprojects of GEMS to carry out a 5-year long reanalysis of atmospheric composition data for the period 2003-2007, assimilating satellite data to constrain O3, CO, CO2, CH4, and aerosol optical depth. It is also being used for a near-real time analysis of O3, CO and aerosol optical depth that is being run at ECMWF. Fields from these analyses are available from http://gems.ecmwf.int/data.jsp

5 Acknowledgements

GEMS was funded by the European Commission under the EU Sixth Research Framework Programme, contract number SIP4-CT-2004-516099.

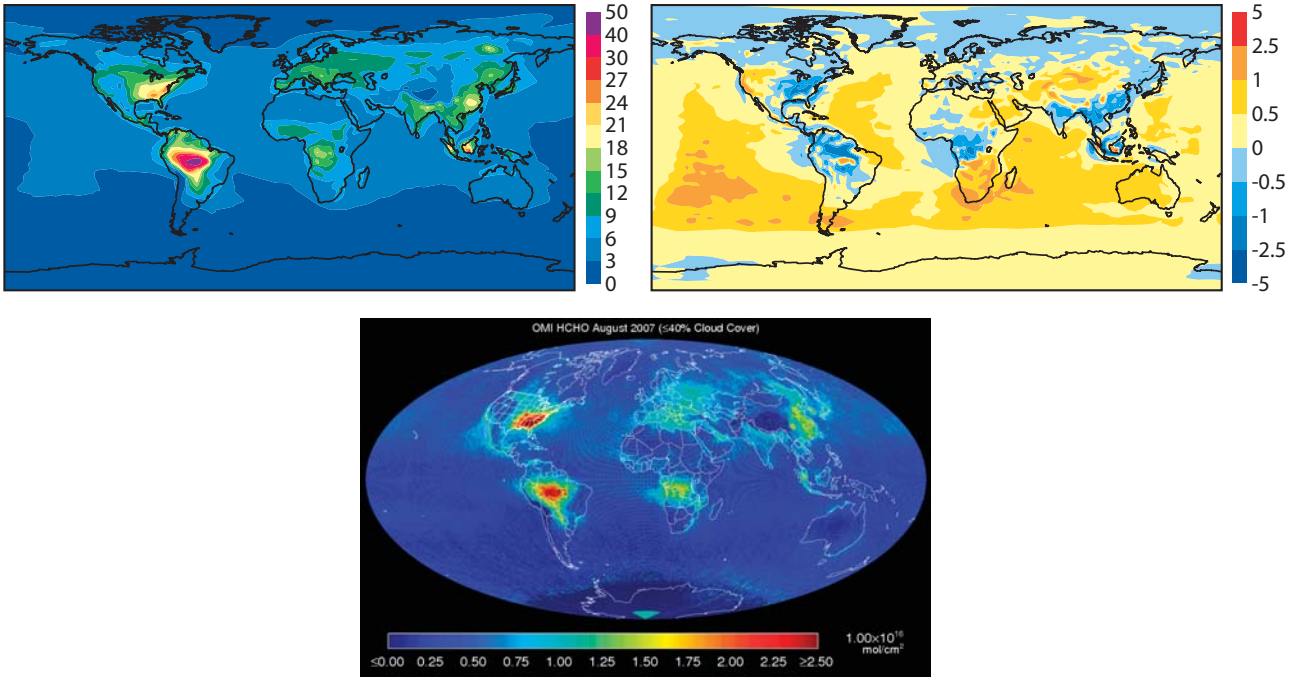

Figure 17: Monthly mean total column HCHO field in $10^{15} mol/cm^2$ from HCHOAN (top left) and the difference between HCHOAN and HCHOCTRL (HCHOAN minus HCHOCTRL) (top right) for August 2007. The bottom panel shows the monthly mean total column HCHO field from OMI, obtained from http://www.cfa.harvard.edu/ tkurosu/SatelliteInstruments/OMI/SampleImages/HCHO/index.html.

6 References

Atkinson, R. (1994): Gas-phase tropospheric chemistry of organic compounds. J. Phys. Chem. Ref. Data Monogr., 2, 13-46.

Benedetti et al. (2009): Aerosol analysis and forecast in the ECMWF Integrated Forecast System: Data assimilation, submitted to J. Geophys. Res..

Boersma, K.F., Eskes, H.J., and Brinksma, E.J. (2004): Error analysis for tropospheric NO_2 retrieval from space.J. Geophys. Res., 109, D04311, doi:10.1029/2003JD003962.

Cariolle, D. and Deque, M. (1986): Southern hemisphere medium-scale waves and total ozone disturbances in a spectral general circulation model. J. Geophys. Res., 91D, 1082510846.

Courtier, P., Thépaut, J.-N. and Hollingsworth, A. (1994): A strategy for operational implementation of 4D-Var, using an incremental approach. Q. J. R. Meteorol. Soc., 120, 1367-1388.

Crutzen, P., and Schmailzl, U. (1983): Chemical budgets of the stratosphere, Planet. Space. Sci., 31, 1009-1020.

Deeter et al. (2003): Operational carbon monoxide retrieval algorithm and selected results for the MOPITT instrument. J. Geophys. Res., 108(D14), 4399, doi:10.1029/2002JD003186

Dethof, A. and Hólm, E.V (2004): Ozone assimilation in the ERA-40 reanalysis project. Quart . J. Roy. Met. Soc., 130, 2851-2872.

De Smedt, I., M"uller, J.F., Stavrakou, T., van der A, R., Eskes, H, and Van Roozendael, M. (2008): Twelve

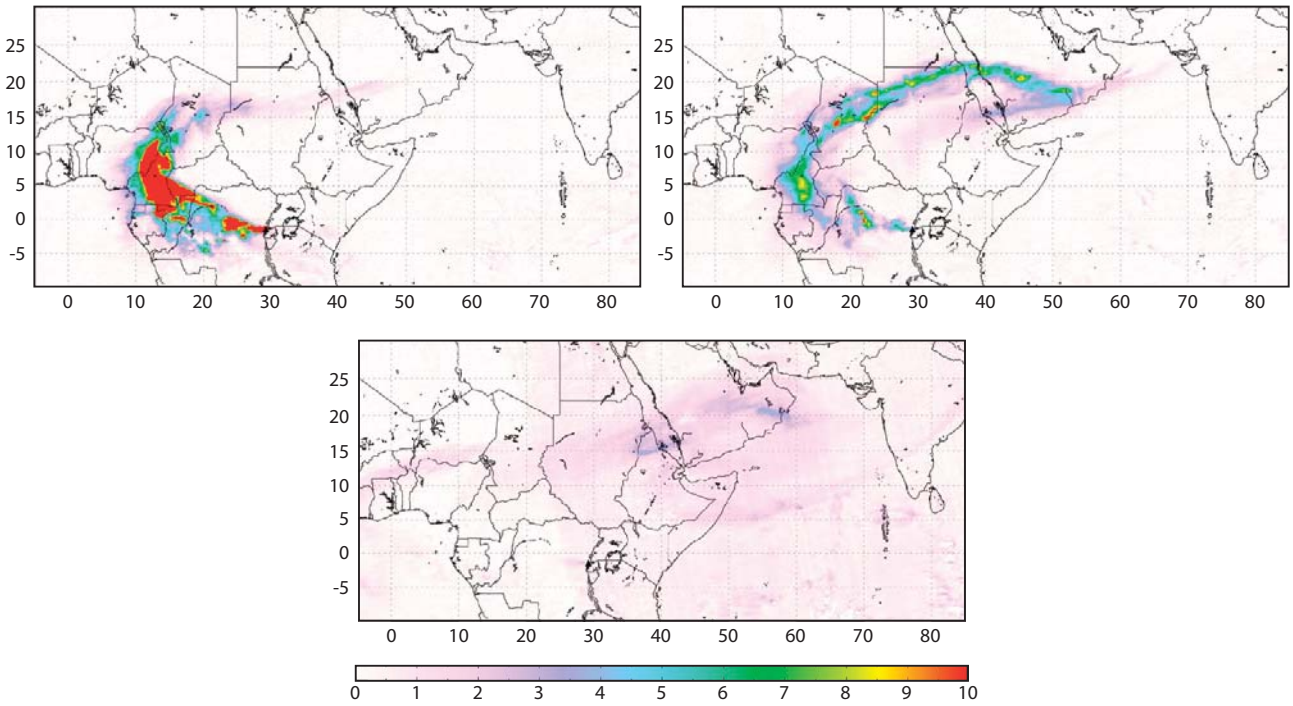

Figure 18: Total column SO_2 field in Dobson Units from OMI on 1, 3, and 6 December 2006. The plots were taken from the OMI Sulfur Dioxide Group website http://so2.umbc.edu/omi/.

years of global observations of formaldehyde in the troposphere using GOME and SCIAMAHCY sensors. Atmos. Chem. Phys., 8, 4947-4963.

Elguindi, N. et al. (2009): Improvment of the global distribution and long-range transport of tropospheric CO by using the IFS-ECMWF model coupled to a free CTM with CO MOPITT assimilation. In preparation.

Engelen R. J., S. Serrar, F. Chevallier (2009), Four-dimensional data assimilation of atmospheric CO2 using AIRS observations, J. Geophys. Res., 114, D03303, doi:10.1029/2008JD010739.

Granli, T., and Bokman, O. (1994): Nitous oxides from agriculture, Nor. J. Acric. Sci., 12, 1-128.

Hansen, J., M. Sato, and R. Ruedy (1997): Radiative forcing and climate response, J. Geophys. Res., 102, 68316864.

Hollingsworth, A., R.J. Engelen, C. Textor, A. Benedetti, O. Boucher, F. Chevallier, A. Dethof, H. Elbern, H. Eskes, J. Flemming, C. Granier, J.W. Kaiser, J.J. Morcrette, P. Rayner, V.H. Peuch, L. Rouil, M.G. Schultz, A.J. Simmons, and The GEMS Consortium (2008): Toward a Monitoring and Forecasting System For Atmospheric Composition: The GEMS Project. Bull. Amer. Meteor. Soc., 89, 11471164, doi:10.1175/2008BAMS2355.1

Hólm, E. V., Untch, A., Simmons, A., Saunders, R., Bouttier, F. and Andersson, E. (1999): Multivariate ozone assimilation in four-dimensional data assimilation. Pp. 89-94 in Proceedings of the SODAWorkshop on Chemical Data Assimilation, 9-10 December 1998, KNMI, De Bilt, The Netherlands.

Horowitz, L. W., Walters, S., Mauzerall, D.L., Emmons, L.K., Rasch, P.J., Granier, C., Tie, X., Lamarque, J.F., Schultz, M.G., Tyndall, G.S., Orlando, J.J. and Brasseur, G.P. (2003): A global simulation of tropospheric ozone and related tracers: Description and evaluation of MOZART, version 2, J. Geophys. Res., doi:10.1029/2002JD002853.

Josse B., Simon P. and V.-H. Peuch (2004) : Rn-222 global simulations with the multiscale CTM MOCAGE,

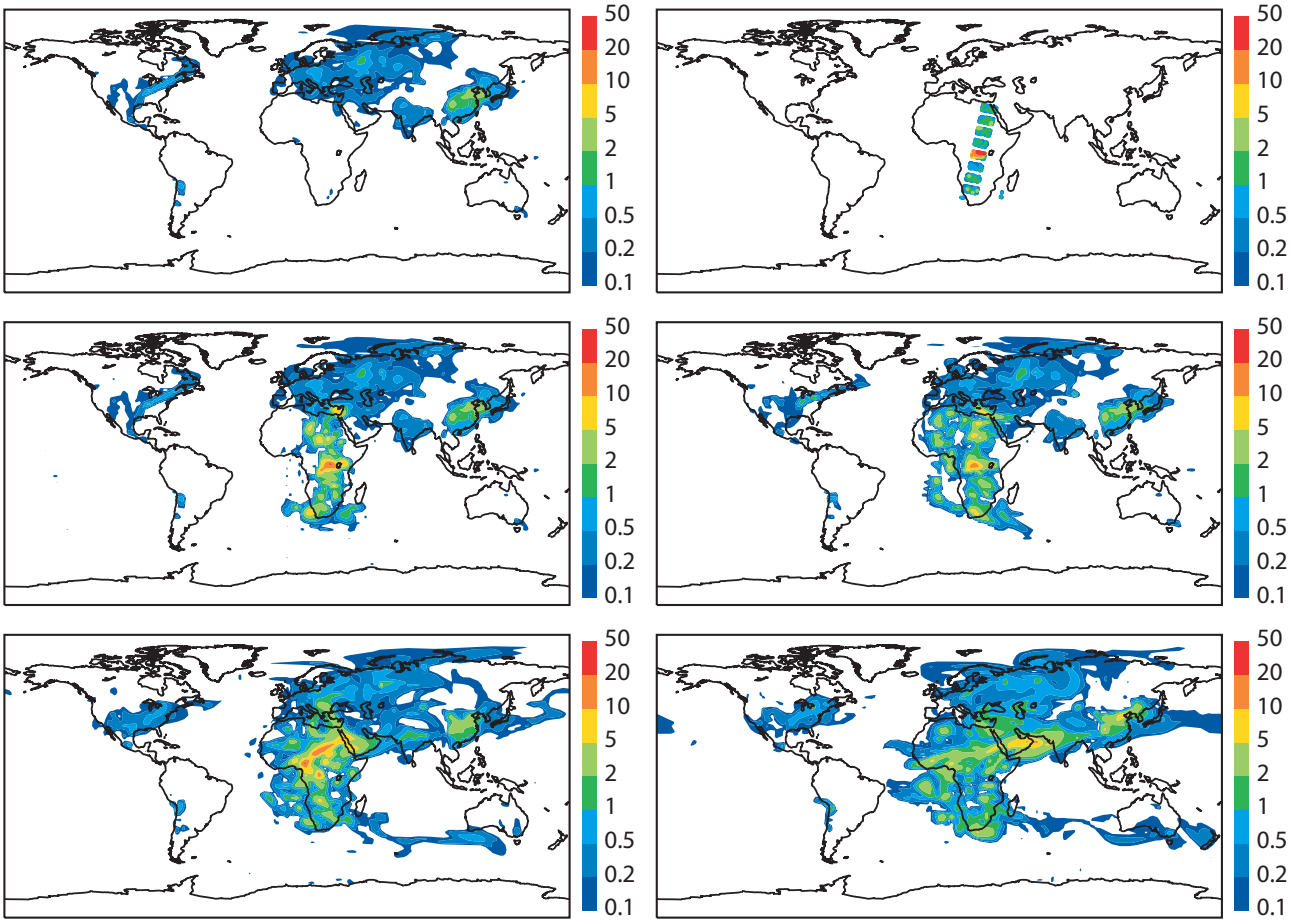

Figure 19: Total column SO_2 field in Dobson Units from SO2AN. Background forecast for 1 Dec, 0z (top left), SCIAMACHY observations that are assimilated in SO2AN on 1 Dec, 0z (top right), SO2 analysis for 1 Dec, 0z (middle left), 1 Dec, 12z (middle right), 3 Dec, 12z (bottom left) and for 6 Dec, 12z (bottom right).

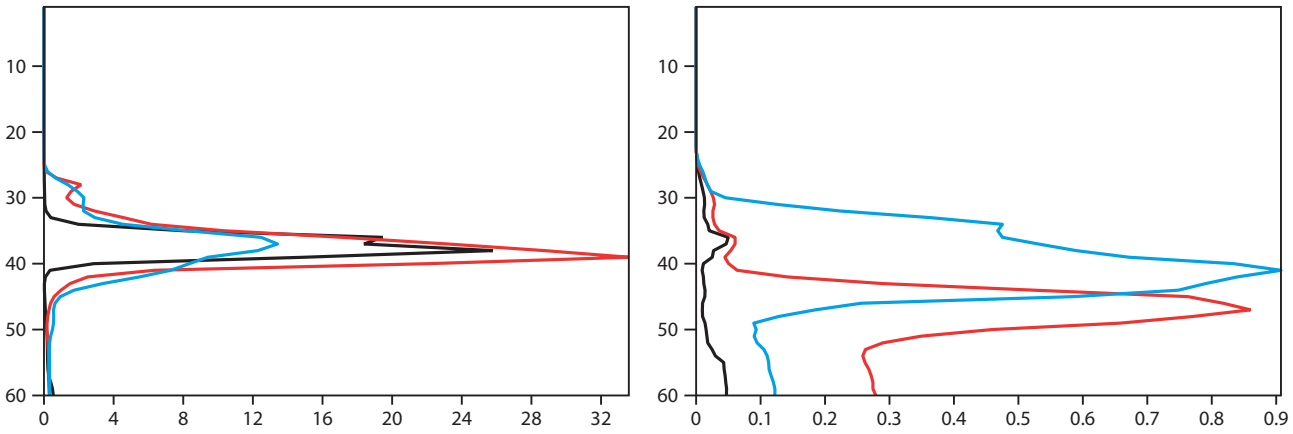

Figure 20: Profiles of SO_2 in ppb averaged over the area between 20°N and 20°S, 0° and 50°E (left) and over the area between 30-40°N, 160-180°E (right), on 20061201, 0z (black), 20061203, 12z (red) and 20061206, 12z (blue).

Tellus, 56B, 339-356.

Fisher, M. and Andersson, E. (2001): Devlopments in 4D-Var and Lalman Filterning. ECMWF Technical Memorandum 347. Available from ECMWF, Shinfield Park, Reading, Berkshire, RG2 9AX, UK.

Fisher, M. (2004): Generalized frames on the sphere with application to background error covariance modellig. Seminar on resent developments in numberical methods for atmospheric and ocean modelling, 6-10 September 2004. Proceedings, ECMWF, pp. 87-101. Available from ECMWF, Shinfield Park, Reading, Berkshire, RG2 9AX, UK.

Fisher, M. (2006): Wavelet Jb - A new way to model the statistics of background errors. ECMWF Newsletter, 106, 23-28. Available from ECMWF, Shinfield Park, Reading, Berkshire, RG2 9AX, UK.

Flemming, J., Inness, A., Flentje, H., Huijen, V., Moinat, P., Schultz, M.G. and Stein O. (2009): Coupling global chemistry transport models to ECMWF's integrated forecast system for forecast and data assimilation. ECMWF Technical Memorandum 590. Available from ECMWF, Shinfield Park, Reading, Berkshire, RG2 9AX, UK.

Hortal, M. and Simmons, A.J. (1991): Use of reduced Gaussian grids in spectral models. Mon. Wea. Rev., 119, 1057-1074

Kanakidou, M., and P. J. Crutzen (1999): The photochemical source of carbon monoxide: Importance, uncertainties, and feedbacks, Chemosphere Global Change Sci., 1, 91109.

Kinnison, D.E., Brasseur, G.P., Walters, S., Gracia, R.R., Marsh, D.R., Sassi, F., Harvey, V.L., Randall, C.E., Emmons, L., Lamarque, J.F., Hess, P., Orlando, J.J., Tie, X.X., Randel, W., Pan, L.L., Gettelman, A., Granier, C., Diehl, T., Niemeier, U. and Simmons, A.J. (2007): Sensitivity of chemical tracers to meteorological parameters in the MOZART-3 chemical transport model. J. Geophys. Res, 112, D20302, doi:10.1029/2006JD007879.

GEMS GRG validation report (2009). Available from http://gems.ecmwf.int/documents/index.jsp.

Kleinman, L., Y.-N. Lee, S. R. Springston, J. H. Lee, L. Nunnermacker, J. Weinstein-Lloyd, X. Zhou, and L. Newman (1995): Peroxy radical concentration and ozone formation rate at a rural site in the southeastern United States, J. Geophys. Res., 100(D4), 7263-7274.

Krol, M.C.,and van Weele, M. (1997): Implications of variations in photodissociation rates for global tropospheric chemistry, Atmospheric environment, 31, 1257-1273.

Krol, M.C., S. Houweling, B. Bregman, M. van den Broek, A. Segers, P. van Velthoven, W. Peters, F. Dentener, and P. Bergamaschi The two-way nested global chemistry-transport zoom model TM5 (2005): algorithm and applications Atmos. Chem. Phys., 5, 417-432.

Landgraf, J. and P.J. Crutzen (1998): An efficient method for online calculations of photolysis and heating rates. J. Atmos. Sci., 55, 863-878.

Logan, J. A., M. J. Prather, S. C. Wofsy, and M. B. McElroy (1981): Tropospheric chemistry: A global perspective, J. Geophys. Res., 86, 72107254.

Lopez, P. and Moreau, E. (2005): A convection scheme for data assimilation: Description and initial tests, Quarterly Journal of the Royal Meteorological Society, 131, 606, p 409-436.

Martin, R. V., B. Sauvage, I. Folkins, C. E. Sioris, C. Boone, P. Bernath, and J. Ziemke (2007): Space-based constraints on the production of nitric oxide by lightning, J. Geophys. Res., 112, D09309, doi:10.1029/2006JD007831.

National Research Council (NRC) (1991): Rethinking the Ozone Problem in Urban and Regional Air Pollution, Natl. Acad. Press, Washington, D. C..

Nedelec, P. et al. (2003): An improved infrared carbon monoxide analyser for routine measurements aboard commercial aircraft: technical validation and first scientific results ofr the MOZAIC III programme, Atmos. Chem. Phys., 3, 1551-1564.

Ordonez, C. et al. (2009): Global model simulations of air pollution during the European 2003 heat wave. In preparation.

Parrish, D.F. and J.C. Derber (1992): The National Meteorological Center's spectral statistical-interpolation analysis scheme. Mon. Weather Rev., 120, 1747-1763

Pham, M., Müller, J.-F., Brasseru, G.P., Garnier, C, and Mégie, G. (1996): A 3D model study of the golbal sulphur cycle: Contibutions fo anthropogenic and biogenic sources, Atmos. Environ., 30, 1815-1822.

Seinfeld, J. H., and S. N. Pandis (2006): Atmospheric Chemistry and Physics: From Air Pollution to Climate Change, John Wiley, Hoboken, N. J.

Stein, O. (2009): Model documentation of the MOZART CTM as implemented in the GEMS system. Available from: http://gems.ecmwf.int/documents/index.jsp#grg.

Valcke, S. and Redler, R. (2006): OASIS4 User Guide (OASIS4_0_2). PRISMSupport Initiative, Technical Report No 4. Available from http://www.prism.enes.org/Publications/index.php.